IEEE Access
Multidisciplinary | Rapid Review | Open Access Journal

Received October 10, 2019, accepted October 25, 2019, date of publication November 4, 2019, date of current version November 15, 2019.

Digital Object Identifier 10.1109/ACCESS.2019.2951429

A Novel Blended State Estimated Adaptive Controller for Voltage and Current Control of Microgrid Against Unknown Noise

MD. SHAHIN MUNSI[1], ABU BAKAR SIDDIQUE[1], SAJAL K. DAS[1], SANJOY KUMAR PAUL[2], MD. RABIUL ISLAM[3], (Senior Member, IEEE), AND MOHAMMAD ALI MONI[4,5]

[1]Department of Mechatronics Engineering, Rajshahi University of Engineering & Technology, Rajshahi 6204, Bangladesh
[2]UTS Business School, University of Technology Sydney, Sydney, NSW 2007, Australia
[3]School of Electrical, Computer and Telecommunications Engineering, University of Wollongong, Wollongong, NSW 2522, Australia
[4]Faculty of Medicine and Health, The University of Sydney, Sydney, NSW 2006, Australia
[5]Department of Computer Science and Engineering, Pabna University of Science & Technology, Pabna 6600, Bangladesh

Corresponding author: Mohammad Ali Moni (mohammad.moni@sydney.edu.au)

ABSTRACT In this study, a novel blended state estimated adaptive controller is designed for voltage and current control of microgrid against unknown noise. The core feature of the microgrid (MG) is its ability to integrate more than one distributed energy resource into the main grid. The state of a microgrid may deteriorate due to many reasons, for example malicious cyber-attacks, disturbances, packet losses, etc. Therefore, it is necessary to achieve the true state of the system to enhance the control requirement and automation of the microgrid. To achieve the true state of a microgrid, this study proposes the use of an algorithm based on the unscented kalman filter (UKF). The proposed state estimator technique is developed using an unscented-transformation and sigma-points measurement technique capable of minimizing the mean and covariance of a nonlinear cost function to estimate the true state of a single-phase, three-phase single-source and three-phase multi-source microgrid system. The advantage of the proposed estimator over using extended kalman filter (EKF) is investigated in simulations. The results demonstrate that the use of the UKF estimator produces a superior estimation of the system compared with the use of the EKF. An adaptive PID controller is also developed and used in system conjunction with the estimator to regulate its voltage and current against the number of loads. Deviation in load parameters hamper the function of the MG system. The performance of the developed controller is also evaluated against number of loads. Results indicate the controller provides a more stable and high-tracking performance with the inclusion of the UKF in the system.

INDEX TERMS Microgrid, model reference adaptive control, state estimation, unscented kalman filter, voltage and current control.

I. INTRODUCTION

In this modern era of technology, the energy crisis and global warming are arguably the most significant issues the world is facing. These issues continue to lead the world to disaster due to the extreme use of oil and coal via typical energy-generation plants. The use of oil and coal is the chief cause of greenhouse gas emission and, thus, the reason for the disasters that ensue [1]–[3]. These energy resources are finite and depleted daily due to increasing demands associated with energy consumption. To attempt to overcome this critical issue, the microgrid concept was introduced. Microgrid technology is an alternative way of producing electric power using distributed energy resources (DERs) like fuel cells, wind turbines, PV arrays and bio-gases [4], [5]. Nowadays, this concept is applied regularly as it involves substantial utilization of renewable energy resources [6]–[8].

Fig. 1 represents a schematic of a commonly used microgrid system. The optimal performance of a microgrid depends on the DER unit. The DER unit is largely used due to its capacity to lessen the use of non-renewable energy resources and, hence, assist in solving the issues associated with energy consumption. This unit also mitigates the emission of methane, carbon dioxide and various oxide gases,

The associate editor coordinating the review of this manuscript and approving it for publication was Giambattista Gruosso.

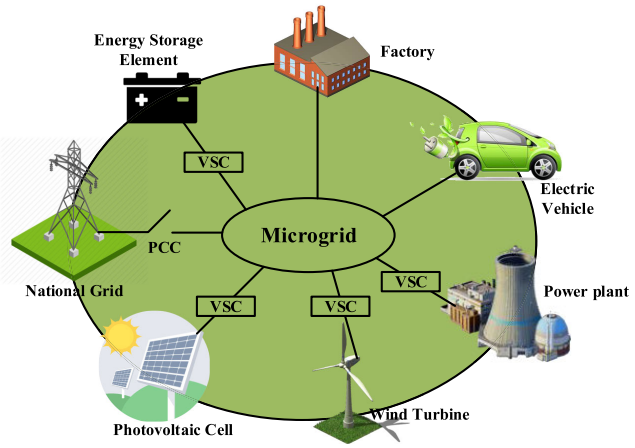

FIGURE 1. Schematic of microgrid system.

in turn reducing the amount of greenhouse gas in the atmosphere [9]–[11]. The proper functioning of DERs depends on various circumstances like wind speed, and solar strength and capacity (among many other factors). Malicious cyber-attacks, packet losses and disturbances may cause variation in factors impacting DERs, introducing noise into the system [12]–[14]. To achieve the best possible outcomes and performance, it is necessary to filter out such noise from the state of the system.

A. MOTIVATION AND INCITEMENT

In this paper, a novel blended state estimated adaptive controller is designed for the control of voltage and current of microgrid (MG). The underlying motivation for this study is to estimate the true state of a microgrid against unknown input and measurement noise. Noise may develop due to an insecure state when voltage and line currents exceed their operational constraints and the power system is still running. This incorrect measurement degrades the microgrid performance from the desired response. To get rid of this problem, the unscented kalman filter (UKF) is designed for estimating the microgrid parameters.

Remark 1: In this work, UKF is used over EKF since, for a nonlinear system, EKF uses Taylor series expansion and Jacobian matrix for linearizing the system which takes more complex calculation in account and when the system is highly nonlinear, it may diverge. Moreover, EKF only considers the mean of the Gaussian for linearizing the system. To overcome these limitations, UKF technique comes in handy as it uses unscented transformation (UT) that includes sigma points of $2K + 1$, including the mean of the Gaussian, where K is the dimension of the system. These sigma points helps to achieve better approximation when the system is highly nonlinear.

The performance of a microgrid can also be compromised under the condition of unknown parameters. These unknown parameters can often be the product of various load dynamics and faults. To minimize these unknown parameters and achieve a high-tracking performance, an adaptive PID controller is designed and integrated along with the UKF.

Scientists are currently working to propose various methods that may filter out this noise then estimate the actual state of the microgrid. Hence, this actual state is used to control the voltage and current efficiently. Accordingly, many filtering algorithm based control strategies were discussed in the earlier literature to estimate this state and control the voltage and current of the grid.

B. LITERATURE REVIEW

The weighted least squares (WLS) estimation method has often been adopted for estimating the state of the microgrid. This method works based on the generalizability of linear regression and ordinary least squares, in which the error covariance matrix differs from the identity matrix, thus minimizing the sum of the squares of the weighted residuals [15]. The major drawback of this WLS algorithm is that it fails to converge the solution due to numerically ill-conditioned gain matrix. This divergence limits the algorithm in terms of its poor estimating the system state, ultimately limiting the use of the WLS method [16].

The extended kalman filter (EKF) is a very popular method in calculating the state estimation of nonlinear systems. This method simultaneously estimates the state of a dynamic system along with its parameters [17]. The propagation of the Gaussian random variable (GRV) is a vital operation in estimating the state. The state distribution in the EKF is approximated using a GRV, which may produce plenty of errors into the true posterior covariance and mean. Moreover, when the system is extremely nonlinear, the EKF does not have the capability to estimate correctly. To overcome this disadvantage, the EKF requires linearized system parameters, which are created using the Jacobian calculation [18].

The distributed kalman filter (DKF) gives a reliable solution for the tracking of the true state in a linear system. This method consists of micro-Kalman filters and also involves a low-pass and band-pass filter [19], [20]. The DKF requires all measurement models to be known; however, it is often very difficult to know all the measurement models. Furthermore, global information is required from the state-error covariance matrix that makes the computation more complex.

The particle filter (PF) is another commonly used estimation algorithm employed in microgrid state estimation. This algorithm was developed for non-Gaussian, as well as nonlinear, systems [21], [22]. Generally speaking, PF is a set of Monte Carlo algorithms in which probabilities are renewed depending on the changing weights and rates of the particles. Therefore, posterior-probability distributions are calculated based on the measurements of particle weights. However, greater computational complexity and poor performance in higher-dimensional spaces limit the application of the PF algorithm.

Least mean squares (LMS) is an iterative algorithm widely used for the state estimation of power systems to overcome the issues associated with the WLS method [23], [24]. The gradient vector is It is an adaptive algorithm capable of estimating the gradient vector from available data. LMS makes

successive corrections to the weight vector in the direction of the negative gradient vector to reduce the mean squares error. It is a relatively simple method because it does not require any calculations for a correlation function or matrix inversion [25]. The main drawback of this estimator is the need for tuning the step-size parameters involved in the calculation. The normalized least mean squares (NLMS) algorithm solves the problem of step-size parameters by normalizing the input signal and then variable step-size LMS algorithm is used to solve the problem of NLMS.

A number of methods have been established for controlling the voltage and current of the microgrid system by ignoring the effect of noise in the form of packet losses and disturbances. Noise may arise in the system due to packet losses, disturbances and cyber-attacks. This phenomena greatly reduces the stability of the microgrid and hence, a noise removing algorithm is needed to be integrated with the controller that will filter out the noise and will provide the actual state to the control unit.

H-infinity controller is a well known control technique used in microgrid for its robust performance and stability [26], [27]. The design of the controller does not guarantee the estimation of noise. It brings robustness to the system with the inclusion of uncertainties. Norm minimizing technique is used to design such controllers. The higher degree control scheme is obtained to handle the higher degree system that makes sure the optimal function with the advanced digital signal processing (DSP) system. Lack of noise estimation and use of the DSP bounds the usage of this controller.

Model predictive control (MPC) technique is another renowned technique that has been applied for microgrid voltage and current regulation using a multi-variable control approach that incorporates the use of a dynamic system and optimizing receding prediction horizon [28], [29]. The main feature of this technique is that it allows the current timeslot to be optimized while keeping future timeslots in an account. Lack of flexibility and uncertainty in the successful translation of mathematical model reduces the application of MPC controller. In addition, filter inclusion for estimating the state is a daunting task for this controller. As a result, noise reduction becomes more complex and may fail to some extent.

Linear quadratic regulator (LQR), designed by linearization technique, is an approach to achieve accurate operation of the microgrid system [30], [31]. The LQR is developed using a mean value theorem. The LQR shows better performance against the parallel RLC networks connected to the grid [32]. Changes in plant dynamics reduces the robustness of the controller and limit the application of it.

C. CONTRIBUTION AND PAPER ORGANIZATION

This paper presents the design of a novel blended state estimated adaptive controller to improve the voltage and current profile for multi DG islanded microgrid against unknown loads and faults. The problem statement of voltage and current control of islanded microgrid has been extended to incorporate the effect of system noise in the form of packet losses and disturbances. Instead of achieving control design for nominal plant model of islanded microgrid such as presented in [33], [34], we propose a new problem statement incorporating the dynamics of system noises that models the perturbed microgrid at noisy operation for islanding mode.

In this work, we present the design of a novel blended state estimated adaptive control technique that firstly estimates the true state of islanded microgrid at noisy situations and provides extensive high performance control of voltage and current for such variations of plant dynamics of the microgrid. The effectiveness of the proposed technique is demonstrated for multi DGs islanded microgrid against plant perturbation due to system noise in the form of packet losses and disturbances, unknown loads and uncertain faults. The results illustrate that the proposed control technique provides robust control and achieve high performance against the number of loads, and faults of the perturbed microgrid.

The work is organised as follows. The model of a single-phase, three-phase, single source and three-phase multi-source microgrid is presented in section II. Section III presents the design of a blended state estimated adaptive controller. The effectiveness of the algorithm is evaluated in section IV and, finally, the conclusion of the paper is presented section V.

II. DESIGN OF MICROGRID

The schematics of the microgrid system used in this study are shown in Fig. 2. The primary units of a microgrid are the voltage source inverter (VSI), where the insulated-gate-bipolar-transistor (IGBT) is used for switching; the LC filter; the transformer; and, finally, the load. The capacitor C_t is used to reduce the load harmonics which is controlled by an internal oscillator at a fixed frequency $\omega_0 = 2\pi f$.

A. SINGLE-PHASE SINGLE-SOURCE MICROGRID

From Fig. 2(a), inductor voltage is

$$\hat{V}_L = L_t \frac{d\hat{I}_L}{dt} \tag{1}$$

Hence

$$\frac{d\hat{I}_L}{dt} = \frac{\hat{V}_L}{L_t} = \frac{\hat{V}_{sw} - \hat{V}_g}{L_t} \tag{2}$$

where, $\hat{I}_L$, $\hat{V}_{sw}$ and $\hat{V}_g$ indicates the inductor current, switching voltage and grid voltage respectively. Transforming (1) and (2) into laplace domain, we get:

$$\hat{V}_L(s) = sL_t\hat{I}_L(s)$$

and

$$\hat{I}_L(s) = \frac{\hat{V}_L(s)}{sL_t} = \frac{\hat{V}_{sw}(s) - \hat{V}_g(s)}{sL_t}$$

Product of supplied dc voltage and duty ratio generates the switching voltage $\hat{V}_{sw}(s)$ as expressed in (3),

$$\hat{V}_{sw}(s) = \alpha(s)\hat{V}_{dc}(s) \tag{3}$$

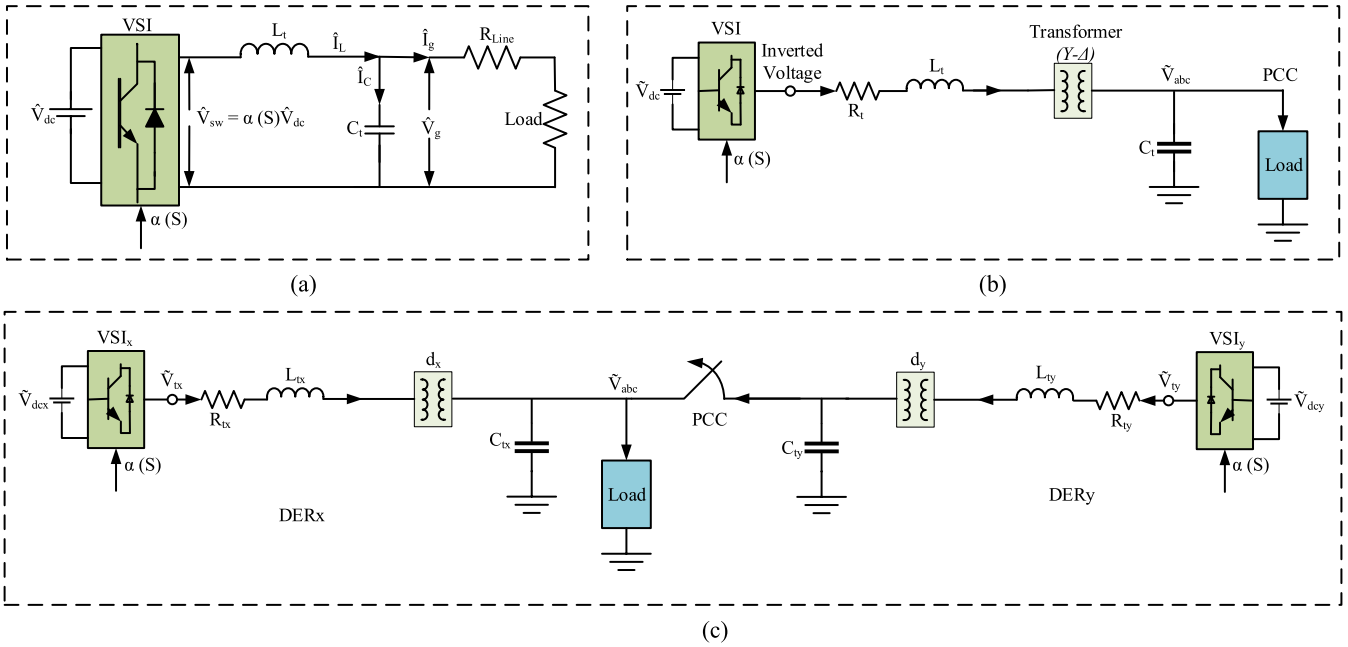

FIGURE 2. Single line diagram of (a) single-phase single-source, (b) three-phase single-source and (c) three-phase multi-source microgrid system.

The grid voltage is obtained as

$$\frac{d\hat{V}_g}{dt} = \frac{1}{C_t}\hat{I}_C = \frac{1}{C_t}(\hat{I}_L - \hat{I}_g) \tag{4}$$

Here, current through the capacitor is represented by $\hat{I}_C$. The generalized state space representation is:

$$\begin{aligned} \dot{\boldsymbol{x}} &= \boldsymbol{A}\boldsymbol{x} + \boldsymbol{B}\boldsymbol{u} \\ \boldsymbol{y} &= \boldsymbol{C}\boldsymbol{x} + \boldsymbol{D}\boldsymbol{u} \end{aligned} \tag{5}$$

From (2) and (4), $\boldsymbol{A} = \begin{bmatrix} 0 & -\frac{1}{L_t} \\ \frac{1}{C_t} & 0 \end{bmatrix}$, $\boldsymbol{B} = \begin{bmatrix} \frac{1}{L_t} \\ 0 \end{bmatrix}$, $\boldsymbol{C} = \begin{bmatrix} 0 & 1 \end{bmatrix}$, $\boldsymbol{D} = 0$, $\boldsymbol{u} = \hat{V}_{sw}$ where $\boldsymbol{x} = \begin{bmatrix} \hat{I}_L \\ \hat{V}_g \end{bmatrix}$ and $\boldsymbol{y} = \begin{bmatrix} 0 \\ \hat{V}_g \end{bmatrix}$.

B. THREE-PHASE SINGLE-SOURCE MICROGRID

A schematic of three phase single source microgrid is presented in Fig. 2(b). The model equations are given as:

$$\frac{d\tilde{I}_{t,abc}}{dt} = -\frac{R_t}{L_t}\tilde{I}_{t,abc} + \frac{1}{L_t}\tilde{V}_{t,abc} - \frac{1}{L_t}\tilde{V}_{abc} \tag{6}$$

and

$$\frac{d\tilde{V}_{abc}}{dt} = \frac{1}{C_t}\tilde{I}_{t,abc} \tag{7}$$

The equation (6) and (7) may be converted into dq frame as follows:

$$\frac{d\tilde{I}_{t,dq}}{dt} = -j\omega_0\tilde{I}_{t,dq} - \frac{R_t}{L_t}\tilde{I}_{t,dq} + \frac{1}{L_t}\tilde{V}_{t,dq} - \frac{1}{L_t}\tilde{V}_{dq} \tag{8}$$

and

$$\frac{d\tilde{V}_{dq}}{dt} = -j\omega_0\tilde{V}_{dq} + \frac{1}{C_t}\tilde{I}_{t,dq} \tag{9}$$

TABLE 1. Parametric values of three-phase single-source microgrid.

Description	Value
DC bus voltage (V_{dc})	2000 V
VSI terminal voltage (V_{base})	600V (1 pu)
Transformer voltage ratio (Y/Δ)	0.6/13.8
PWM carrier frequency (f_{sw})	1980 Hz
System frequency (f_0)	60 Hz
VSI filter resistance (R_t)	1.5$m\Omega$
DG rated power (S_{base})	3 MVA(1 pu)
VSI filter inductance (L_t)	100 μH
VSI filter capacitance (C_t)	100 μF
Load resistance (R)	4.33 Ω
Load inductance (L)	100 mH
Load capacitance (C)	1 pF

From (8) and (9), $\boldsymbol{A} = \begin{bmatrix} 0 & \omega_0 & \frac{1}{C_t} & 0 \\ -\omega_0 & 0 & 0 & \frac{1}{C_t} \\ -\frac{1}{L_t} & 0 & -\frac{R_t}{L_t} & \omega_0 \\ 0 & -\frac{1}{L_t} & \omega_0 & -\frac{R_t}{L_t} \end{bmatrix}$, $\boldsymbol{B} = \begin{bmatrix} 0 & 0 \\ 0 & 0 \\ \frac{1}{L_t} & 0 \\ 0 & \frac{1}{L_t} \end{bmatrix}$, $\boldsymbol{C} = \begin{bmatrix} 1 & 0 & 0 & 0 \\ 0 & 1 & 0 & 0 \end{bmatrix}$ and $\boldsymbol{D} = 0$ where $\boldsymbol{x} = \begin{bmatrix} \tilde{V}_d & \tilde{V}_q & \tilde{I}_{t,d} & \tilde{I}_{t,q} \end{bmatrix}^T$, $\boldsymbol{u} = \begin{bmatrix} \tilde{V}_{t,d} & \tilde{V}_{t,q} \end{bmatrix}^T$ and $\boldsymbol{y} = \begin{bmatrix} \tilde{V}_d & \tilde{V}_q \end{bmatrix}$. The parametric values of three phase single source microgrid is given in Table 1.

TABLE 2. Parametric values of three-phase multi-source microgrid.

Symbols	Value	Symbols	Value
R_{tx}	$1.2 \times 10^{-3}\Omega$	R_{xy}	1.2Ω
R_{ty}	$1.6 \times 10^{-3}\Omega$	R_{yx}	1.2Ω
C_{tx}	$62.86 \times 10^{-6}F$	C_{ty}	$76 \times 10^{-6}F$
L_{tx}	$93.7 \times 10^{-6}H$	L_{xy}	$94.8 \times 10^{-6}H$
L_{ty}	$94.8 \times 10^{-6}H$	L_{yx}	$104.3 \times 10^{-6}H$
f_0	$60Hz$	d_x	$0.6/13.8(Y-\Delta)$
Q	$0.001 * I$	R	0.2
V_{dc}	$2000V$	Δt	0.000001

C. THREE-PHASE MULTI-SOURCE MICROGRID

A schematic of a three-phase multi-source microgrid is shown in Fig. 2(c). Two DERs are connected by point of common coupling (PCC). The dynamics of the system may be written as follows:

For DERx:

$$\dot{\tilde{V}}_{x,dq} = -j\omega_0\tilde{V}_{x,dq} + (d_x\tilde{I}_{tx,dq} + \tilde{I}_{xy,dq})/C_{tx} \quad (10)$$

$$\dot{\tilde{I}}_{tx,dq} = -j\omega_0\tilde{I}_{tx,dq} - (d_x\tilde{V}_{x,dq} + R_{tx,dq}\tilde{I}_{tx,dq} - \tilde{V}_{tx,dq})/L_{tx} \quad (11)$$

For DERy:

$$\dot{\tilde{V}}_{y,dq} = -j\omega_0\tilde{V}_{y,dq} + (d_y\tilde{I}_{ty,dq} + \tilde{I}_{yx,dq})/C_{ty} \quad (12)$$

$$\dot{\tilde{I}}_{ty,dq} = -j\omega_0\tilde{I}_{ty,dq} - (d_y\tilde{V}_{y,dq} + R_{ty,dq}\tilde{I}_{ty,dq} - \tilde{V}_{ty,dq})/L_{ty} \quad (13)$$

For line xy:

$$\dot{\tilde{I}}_{xy,dq} = -j\omega_0\tilde{I}_{xy,dq} + (\tilde{V}_{y,dq} - R_{xy,dq}\tilde{I}_{xy,dq} - \tilde{V}_{x,dq})/L_{xy} \quad (14)$$

For line yx:

$$\dot{\tilde{I}}_{yx,dq} = -j\omega_0\tilde{I}_{yx,dq} + (\tilde{V}_{x,dq} - R_{yx,dq}\tilde{I}_{yx,dq} - \tilde{V}_{y,dq})/L_{yx} \quad (15)$$

Using (10) to (15), the continuous time state space representation for multi-DG based microgrid system is given as $\boldsymbol{A}$ and $\boldsymbol{B}$, shown at the bottom of the next page, where, $\boldsymbol{x} = [\tilde{V}_{x,d}, \tilde{V}_{x,q}, \tilde{I}_{tx,d}, \tilde{I}_{tx,q}, \tilde{I}_{xy,d}, \tilde{I}_{xy,q}, \tilde{I}_{yx,d}, \tilde{I}_{yx,q}, \tilde{V}_{y,d}, \tilde{V}_{y,q}, \tilde{I}_{ty,d}, \tilde{I}_{ty,q}]^T$ and $\boldsymbol{u} = [\tilde{V}_{tx,d}, \tilde{V}_{tx,q}, \tilde{V}_{ty,d}, \tilde{V}_{ty,q}]^T$. The parametric values of three-phase multi-source smart grid is given in Table 2.

III. UNSCENTED KALMAN FILTER ALGORITHM AND CONTROLLER DESIGN

A. UKF ALGORITHM

Since the practical system involves non-linearities, estimation for the non linear system is must in many cases. Although EKF is the most popular method, it shows many limitations for non linear system (see Remark 1). To overcome the limitations, UKF algorithm has been proposed. The implementation of unscented kalman filter for both open-loop and closed-loop system is illustrated in Fig. 3(a) and 3(b) respectively. Here, $\boldsymbol{w_1}, \boldsymbol{w_2}, \ldots, \boldsymbol{w_i}$ represents the weighting matrix of the input noise, whereas, $\boldsymbol{n_1}, \boldsymbol{n_2}, \ldots, \boldsymbol{n_j}$ represents for measurement noise. UKF is a non-linear technique that uses sigma points and unscented transformation to calculate the mean and covariance of the parameter.

The principle of the UT is as follows:

At first the sigma points are choosen from the input distribution. Then transform the sigma points through the non linear function to produce a new set of sigma points belonging to the output distribution. Compute the weighted mean and covariance of the transform sigma points.

Consider a discrete time nonlinear system where the state observation is described as follows:

$$\boldsymbol{x}(\ell+1) = f[\boldsymbol{x}(\ell), \boldsymbol{u}(\ell), \boldsymbol{w}(\ell)] \quad (16)$$

$$\boldsymbol{y}(\ell) = h[\boldsymbol{x}(\ell), \boldsymbol{u}(\ell), \boldsymbol{n}(\ell)] \quad (17)$$

Here, $\boldsymbol{x}(\ell)$ is the state vector, $\boldsymbol{u}(\ell)$ is the input matrix, $\boldsymbol{w}(\ell)$ is the process noise matrix and $\boldsymbol{n}(\ell)$ is the measurement noise matrix of the system. The algorithm of UKF is described as follows:

1) INITIALIZATION

The estimation of $\hat{\boldsymbol{x}}$ at a time step ℓ is represented by $\hat{\boldsymbol{x}}_\ell$. The general equations for the UKF estimation $\hat{\boldsymbol{x}}_\ell$ and covariance $\bar{\boldsymbol{P}}_\ell$ are written as follows (At initial condition $\ell = 0$):

$$\hat{\boldsymbol{x}}_0 = \bar{E}\{\boldsymbol{x}_0\} \quad (18)$$

$$\bar{\boldsymbol{P}}_0 = \bar{E}\{(\boldsymbol{x}_0 - \hat{\boldsymbol{x}}_0)(\boldsymbol{x}_0 - \hat{\boldsymbol{x}}_0)^T\} \quad (19)$$

2) SIGMA POINT CALCULATION

This section describes how to calculate $2K + 1$ weighted sigma points, where K denotes the dimension of $\hat{\boldsymbol{x}}_\ell$. A matrix $\boldsymbol{\chi}$ of $2K + 1$ sigma vectors $\boldsymbol{\chi}^i$ are calculated as follows:

$$\boldsymbol{\chi}^0(\ell-1) = \hat{\boldsymbol{x}}(\ell); \quad i = 0 \quad (20)$$

$$\boldsymbol{\chi}^i(\ell-1) = \hat{\boldsymbol{x}}(\ell-1) + (\sqrt{(K+\lambda)\bar{\boldsymbol{P}}(\ell-1)})_i; \quad i = 1, 2, \ldots, K \quad (21)$$

$$\boldsymbol{\chi}^i(\ell-1) = \hat{\boldsymbol{x}}(\ell-1) - (\sqrt{(K+\lambda)\bar{\boldsymbol{P}}(\ell-1)})_i; \quad i = K+1, K+2, \ldots, 2K \quad (22)$$

where, $(\sqrt{(K+\lambda)\bar{\boldsymbol{P}}(\ell-1)})_i$ is the i^{th} row of the square root matrix. These sigma vectors are propagated through the non-linear function

$$\bar{\boldsymbol{Y}} = f(\boldsymbol{\chi}^i); \quad i = 0, \ldots, 2K \quad (23)$$

The weights of the matrix $\boldsymbol{W}$ are calculated as follows:

$$\boldsymbol{W}_0^m = \frac{\lambda}{(K+\lambda)} \quad (24)$$

$$\boldsymbol{W}_0^c = \frac{\lambda}{(K+\lambda)} + (1 - \alpha^2 + \beta) \quad (25)$$

$$\boldsymbol{W}_i^m = \frac{1}{2(K+\lambda)}; \quad i = 0, \ldots, 2K \quad (26)$$

where $\lambda = \alpha^2(K+\kappa) - K$ is a scaling parameter, α determines the spread of the sigma points around the mean state value and is usually kept to a small positive value, κ is a secondary

scaling parameter that is kept to zero, β incorporates the prior knowledge of the distribution and the optimal value of β is 2. Hence the sigma vector is:

$$\boldsymbol{\chi}(\ell-1) = \left[\hat{\boldsymbol{x}}(\ell-1) \;\; \hat{\boldsymbol{x}}(\ell-1) \pm \left(\sqrt{(K+\lambda)\bar{\boldsymbol{P}}(\ell-1)}\right)_i\right] \quad (27)$$

3) PREDICTION

To propagate the state from time $(\ell-1)$ to time ℓ, unscented transform is applied using the current best guess for mean and covariance. The posterior mean $\bar{\boldsymbol{x}}$ and covariance $\bar{\boldsymbol{P}}_x$ are determined as follows:

$$\bar{\boldsymbol{x}} = \sum_{i=0}^{2K} \boldsymbol{W}_i^m \boldsymbol{\chi}^i \quad (28)$$

$$\bar{\boldsymbol{P}} = \sum_{i=0}^{2K} \boldsymbol{W}_i^c (\boldsymbol{\chi}^i - \bar{\boldsymbol{x}})(\boldsymbol{\chi}^i - \bar{\boldsymbol{x}})^T \quad (29)$$

$$\bar{\boldsymbol{x}}(\ell|\ell-1) = \sum_{i=0}^{2K} \boldsymbol{W}_i^m \boldsymbol{\chi}^i(\ell-1) \quad (30)$$

The approximated covariance calculated by using posterior mean and weighted matrices are given as follows:

$$\bar{\boldsymbol{P}}(\ell|\ell-1) = \sum_{i=0}^{2K} \boldsymbol{W}_i^c (\boldsymbol{\chi}^i(\ell|\ell-1) - \bar{\boldsymbol{x}}(\ell|\ell-1))(\boldsymbol{\chi}^i(\ell|\ell-1) - \bar{\boldsymbol{x}}(\ell|\ell-1))^T + \boldsymbol{Q}(\ell-1) \quad (31)$$

$$\boldsymbol{y}^i(\ell|\ell-1) = h(\ell)(\boldsymbol{x}^i(\ell-1)) \quad (32)$$

$$\bar{\boldsymbol{Y}}(\ell|\ell-1) = \sum_{i=0}^{2K} \boldsymbol{W}_i^m \boldsymbol{y}^i(\ell|\ell-1) \quad (33)$$

4) UPDATING

The innovation covariance ($\bar{\boldsymbol{P}}_{yy}$) and cross covariance ($\bar{\boldsymbol{P}}_{xy}$) matrices are calculated to obtain the kalman gain (K_ℓ) that is used to calculate the corrected mean and covariance.

$$\bar{\boldsymbol{P}}_{yy} = \sum_{i=0}^{2K} \boldsymbol{W}_i^c (\boldsymbol{y}^i(\ell|\ell-1) - \bar{\boldsymbol{Y}}(\ell|\ell-1))(\boldsymbol{y}^i(\ell|\ell-1) - \bar{\boldsymbol{Y}}(\ell|\ell-1))^T + \boldsymbol{R}(\ell) \quad (34)$$

$$\boldsymbol{A} = \begin{bmatrix}
0 & \omega_0 & \frac{d_x}{C_t x} & 0 & \frac{1}{C_{tx}} & 0 & 0 & 0 & 0 & 0 & 0 & 0 \\
\omega_0 & 0 & 0 & \frac{d_x}{C_{tx}} & 0 & \frac{1}{C_{tx}} & 0 & 0 & 0 & 0 & 0 & 0 \\
\frac{-d_x}{L_{tx}} & 0 & \frac{-R_{tx}}{L_{tx}} & \omega_0 & 0 & 0 & 0 & 0 & 0 & 0 & 0 & 0 \\
0 & \frac{-d_x}{L_{tx}} & -\omega_0 & \frac{-R_{tx}}{L_{tx}} & 0 & 0 & 0 & 0 & 0 & 0 & 0 & 0 \\
\frac{1}{L_{xy}} & 0 & 0 & 0 & \frac{-R_{xy}}{L_{xy}} & \omega_0 & 0 & 0 & \frac{1}{L_{xy}} & 0 & 0 & 0 \\
0 & \frac{-1}{L_{xy}} & 0 & 0 & -\omega_0 & \frac{-R_{xy}}{L_{xy}} & 0 & 0 & 0 & \frac{1}{L_{xy}} & 0 & 0 \\
\frac{1}{L_{xy}} & 0 & 0 & 0 & 0 & 0 & \frac{-R_{yx}}{L_{yx}} & \omega_0 & \frac{-1}{L_{yx}} & 0 & 0 & 0 \\
0 & \frac{1}{L_{yx}} & 0 & 0 & 0 & 0 & -\omega_0 & \frac{-R_{yx}}{L_{yx}} & 0 & \frac{-1}{L_{yx}} & 0 & 0 \\
0 & 0 & 0 & 0 & 0 & 0 & \frac{1}{C_{ty}} & 0 & 0 & \omega_0 & \frac{d_y}{C_{ty}} & 0 \\
0 & 0 & 0 & 0 & 0 & 0 & 0 & \frac{1}{C_{ty}} & -\omega_0 & 0 & 0 & \frac{d_y}{C_{ty}} \\
0 & 0 & 0 & 0 & 0 & 0 & 0 & 0 & \frac{-d_y}{L_{ty}} & 0 & \frac{-R_{ty}}{L_{ty}} & \omega_0 \\
0 & 0 & 0 & 0 & 0 & 0 & 0 & 0 & 0 & \frac{-d_y}{L_{ty}} & -\omega_0 & \frac{-R_{ty}}{L_{ty}}
\end{bmatrix}$$

$$\boldsymbol{B} = \begin{bmatrix}
0 & 0 & \frac{1}{L_{tx}} & 0 & 0 & 0 & 0 & 0 & 0 & 0 & 0 & 0 \\
0 & 0 & 0 & \frac{1}{L_{tx}} & 0 & 0 & 0 & 0 & 0 & 0 & 0 & 0 \\
0 & 0 & 0 & 0 & 0 & 0 & 0 & 0 & 0 & 0 & \frac{1}{L_{ty}} & 0 \\
0 & 0 & 0 & 0 & 0 & 0 & 0 & 0 & 0 & 0 & 0 & \frac{1}{L_{ty}}
\end{bmatrix}^T$$

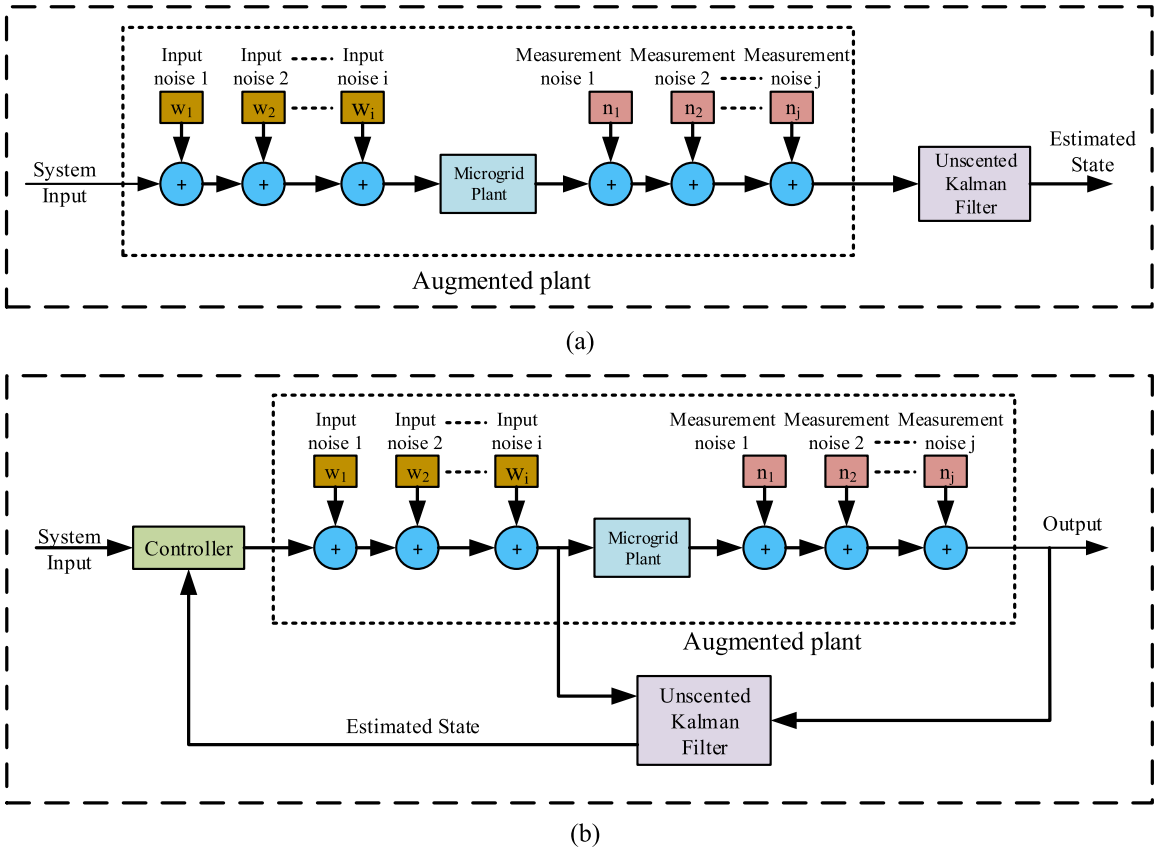

FIGURE 3. (a) Augmented open-loop system and (b) closed-loop system.

$$\bar{\boldsymbol{P}}_{xy} = \sum_{i=0}^{2K} \boldsymbol{W}_i^c (\boldsymbol{x}^i(\ell|\ell-1) - \bar{\boldsymbol{x}}(\ell|\ell-1))(\boldsymbol{y}^i(\ell|\ell-1) - \bar{\boldsymbol{Y}}(\ell|\ell-1))^T \tag{35}$$

Using the above innovation covariance and cross covariance, the kalman gain (K_ℓ) is calculated as follows:

$$K_\ell = \boldsymbol{P}_{xy}\boldsymbol{P}_y^{-1} \tag{36}$$

$$\hat{\boldsymbol{x}}(\ell) = \bar{\boldsymbol{x}}(\ell) + K_\ell(\boldsymbol{y}^{(i)}(\ell|\ell-1) - \bar{\boldsymbol{Y}}(\ell|\ell-1)) \tag{37}$$

$$\hat{\boldsymbol{P}}(\ell) = \hat{\boldsymbol{P}} - K_\ell \hat{\boldsymbol{P}}_{yy} K_\ell{}^T \tag{38}$$

Using the equations (37) and (38) the actual distribution function for nonlinear system can be obtained.

B. CONTROLLER DESIGN

The innovation and design procedures of a multi-operating model-reference based modified-adaptive PID controller for microgrid voltage and current regulation are carried out in this section. Fig. 4 shows the basic structure of the control scheme. A collection of adaptable parameters form the basic structure of the controller. These adaptable parameters play a vital role in the tracking of plant model output close to the reference model output.

The composition of the controller is based on four components: 1. reference model; 2. control section; 3. plant; and 4. adaptive mechanism. The reference model is an important part of this scheme, ensuring the high tracking display of the controller, and hence, it is selected in a way that generates the desired trajectory signal. The control unit is a collection of adaptable parameters and in this paper, parameter ϑ, which is adaptation gain dependent, is employed to generate the control action. The control action is generated from the control unit by comparing the input and output of the plant, with the assistance of adaptation gain.

Another important part of the scheme is the adaptive mechanism. This is used to ensure the high tracking of the ideal plant with respect to the reference model. This mechanism may be evaluated using numerous rules, such as the MIT rule, Lyapunov theory, augmented error theory, etc. In this study, the MIT rule is considered for the evaluation of the adaptive mechanism.

The tracking error ($\mathring{e}$) is calculated from the difference between plant (y_p) and reference model (y_m) output.

$$\mathring{e} = y_p - y_m \tag{39}$$

The controller is designed for a closed-loop system for plant response adjustment close to the reference signal against the unknown parameters. Using (39), the cost function $j(\vartheta)$ is calculated as follows where j is a

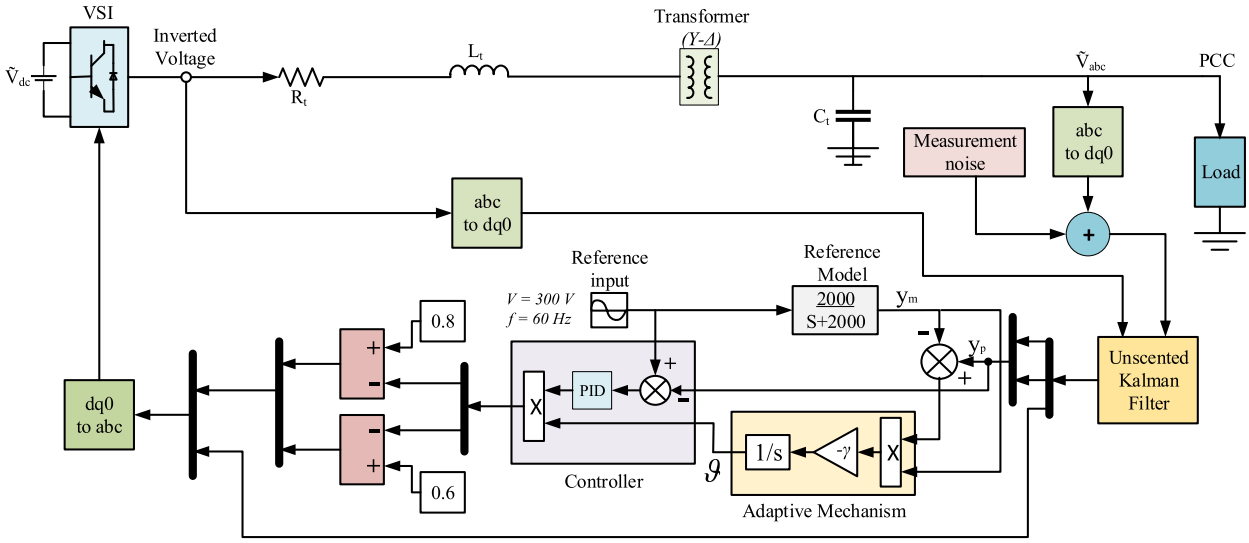

FIGURE 4. Closed-loop control technique of blended state estimated adaptive PID controller.

function of ϑ.

$$j(\vartheta) = \frac{\mathring{e}^2(\vartheta)}{2} \tag{40}$$

here parameter ϑ is determined in a manner that the cost function is minimized to zero. It is done by taking the change in ϑ as directly proportional to the change in the negative slope of j.

$$\frac{d\vartheta}{dt} = -\gamma \frac{\delta j}{\delta \vartheta} = -\gamma\, \mathring{e}\, \frac{\delta \mathring{e}}{\delta \vartheta} \tag{41}$$

where $\frac{\delta \mathring{e}}{\delta \vartheta}$ is a coefficient term and is named as derivative of sensitivity. The interconnection among cost function and derivative of ϑ is referred to as the MIT rule. The adjustable controller gain is determined by a positive amount of γ.

$$j(\vartheta) = |\,\mathring{e}(\vartheta)| \tag{42}$$

$$\frac{d\vartheta}{dt} = -\gamma\, \mathring{e}\, \frac{\delta \mathring{e}}{\delta \vartheta} sign(\mathring{e}) \tag{43}$$

where

$$sign(\mathring{e}) = \begin{cases} 1, & \mathring{e} > 0 \\ 0, & \mathring{e} = 0 \\ -1, & \mathring{e} < 0 \end{cases} \tag{44}$$

Consider that it is a linear approach with a transfer function of $mG(s)$, where $G(s)$ and m are a 2^{nd} order known transfer function and unknown parameters, respectively. The controller design is done in a way that the reference is tracked by the controller with a transfer function of $\frac{Y(s)}{U(s)} = m_0 G(s)$, where m_0 represents a known parameter. From (39), we get

$$\begin{aligned} \mathring{e} &= y_p - y_m \\ &= mG\vartheta U - m_0 GU \end{aligned} \tag{45}$$

Now the update rule is,

$$\frac{\delta \mathring{e}}{\delta \vartheta} = mGU = \frac{m}{m_0} y_m \tag{46}$$

From (43), the formula is given

$$\frac{d\vartheta}{dt} = -\gamma' \frac{m}{m_0} y_m\, \mathring{e} = -\gamma y_m\, \mathring{e} \tag{47}$$

(47) is the updated MIT law, where γ is a positive amount indicating the adaptation gain of the controller and employed to describe the rule associated with the adjusting parameter ϑ.

With the inclusion of MIT law, a second order system is considered to evaluate the effectiveness of the technique. In the control unit, a PID controller is integrated and the transfer function of this is given as follows:

$$C(s) = \frac{k_d s^2 + k_p s + k_i}{s} \tag{48}$$

The transient response is improved by the proportional gain (k_p), steady-state error is reduced by the integral gain (k_i), and the system's overshoot is reduced by the derivative gain (k_d.). In this study, controller gain k_p, k_i and k_d is considered as 135, 12 and 2 respectively and they are governed using trial-and-error technique. To assure high robustness, efficiency, and tracking performance, another gain called adaptation gain (γ), deduced in (47), is determined as 0.001.

C. STABILITY ANALYSIS

The theoretical stability analysis for the proposed controller using the Lyapunov theory is described in this section. Fig. 5 represents the schematic diagram of the model reference adaptive control system.

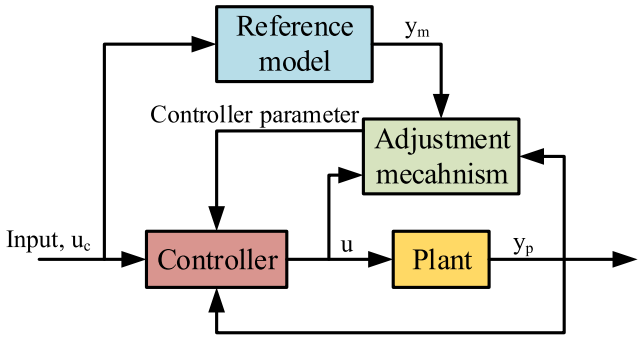

FIGURE 5. Schematic of model reference adaptive control.

Let, for a model reference modified adaptive PID controller, the control law be-

$$u = M_I x_I + M^T x_p \tag{49}$$

For simplicity, consider $M = \begin{bmatrix} M_I & M^T \end{bmatrix}$ and $x_p = \begin{bmatrix} x_I \\ x_p \end{bmatrix}$. Therefore, the control law become $u_c = Mx_p$. The plant model equation,

$$\dot{x}_p = Ax_p + Bu_c \tag{50}$$

and reference model,

$$\dot{x}_m = A_m x_m + B_m u_c \tag{51}$$

For closed-loop system,

$$\begin{aligned} \dot{x}_p &= Ax_p + Bu_c \\ &= Ax_p + BMx_p \\ \dot{x}_p &= (A + BM)x_p \end{aligned} \tag{52}$$

Applying matching condition in (51) and (52), we get $A_m = A + BM$.
Putting the value of M and x_p in (52), we obtain,

$$\begin{aligned} \dot{x}_p &= (A + B\begin{bmatrix} M_I & M^T \end{bmatrix})\begin{bmatrix} x_I \\ x_p \end{bmatrix} \\ &= (Ax_I + Ax_p) + BM_I x_I + BM^T x_p \\ &= (A + BM^T)x_p + (A + BM_I)x_I \end{aligned} \tag{53}$$

The integral state for integral action is taken as $\dot{x}_I = x_p + u_c$. Hence, the closed-loop system is,

$$\begin{bmatrix} \dot{x}_I \\ \dot{x}_p \end{bmatrix} = \begin{bmatrix} 0 & 1 \\ A + BM_I & A + BM^T \end{bmatrix}\begin{bmatrix} x_I \\ x_p \end{bmatrix} + \begin{bmatrix} 1 \\ 0 \end{bmatrix} u_c \tag{54}$$

Applying additional matching condition:
$\bar{A}_m = \begin{bmatrix} 0 & 1 \\ A + BM_I & A + BM^T \end{bmatrix}$ and $B_m = \begin{bmatrix} 1 \\ 0 \end{bmatrix} = B$.
Tracking error, $e = x_p - x_m$. Taking the differentiation of e, we get,

$$\begin{aligned} \dot{e} &= \dot{x}_p - \dot{x}_m \\ &= (A + BM)x_p - A_m x_m - B_m u_c \\ &= A_m x_p - A_m x_m - B_m M x_p \\ &= A_m(x_p - x_m) - B_m M x_p \\ &= A_m e - B_m M x_p \end{aligned} \tag{55}$$

Lyapunov function,

$$V(e, M) = e^T Pe + tr(M^T \Gamma^{-1} M) \tag{56}$$

where P satisfies the Lyapunov equation $PA_m + A_m^T P = -Q$. Differentiating $V(e, M)$, we get,

$$\begin{aligned} \dot{V}(e, M) &= e^T P\dot{e} + \dot{e}^T Pe + tr(M^T \Gamma^{-1}\dot{M}) + tr(\dot{M}^T \Gamma^{-1} M) \\ &= e^T P(A_m e - B_m M x_p) + (A_m^T e^T - B_m^T M^T x_p^T)Pe \\ &\quad + tr(M^T \Gamma^{-1}\dot{M}) + tr(\dot{M}^T \Gamma^{-1} M) \\ &= e^T (PA_m + A_m^T P)e - 2e^T PB_m M x_p + 2tr(\dot{M}^T \Gamma^{-1} M) \\ &= -e^T Qe - 2e^T PB_m M x_p + 2tr(\dot{M}^T \Gamma^{-1} M) \end{aligned} \tag{57}$$

To make $\dot{V} = -e^T Qe$

$$\dot{M}^T = -e^T PB_m \Gamma x_p \tag{58}$$

Putting the value of M, x_p and B_m, we get,

$$\begin{bmatrix} \dot{M}_I \\ \dot{M}^T \end{bmatrix} = -\Gamma \begin{bmatrix} x_I \\ x_p \end{bmatrix} e^T PB \tag{59}$$

Here, the plant state is denoted by x_p and adaptation gain matrix is denoted by Γ which is positive definite and signify the stability of the closed loop system.

IV. PERFORMANCE EVALUATION

A. UNSCENTED KALMAN FILTER PERFORMANCE

The performance of the proposed estimator is given here. The evaluation is done for the single-phase, three-phase single-source and three-phase, multi source microgrid system. The investigation was performed using MATLAB / Simulation software. The simulation outcomes proof that the proposed UKF estimator has the ability to reduce the disturbances from the system, as well as providing a better estimation when compared with the EKF.

1) UKF PERFORMANCE FOR A SINGLE-PHASE SINGLE-SOURCE MICROGRID

The UKF is designed for both voltage and current estimation in a single-phase microgrid system. The voltage estimation for the grid is shown in Fig. 6(a) and the inductor current estimation is shown in Fig. 6(b). From this figure, it is seen that the UKF estimator has the ability to reduce the amount of noise present in the system and provides the estimation close to the true state of the microgrid system. A comparative analysis between the UKF and EKF is presented in Fig. 7(a) and 7(b). This figure ensures a better estimation results of the novel UKF estimator better than the EKF. The error produced by these two filters is also shown in Fig. 7(c) and 7(d), and from this figure it is observed the amount of error produced by the UKF is much lower than that of the EKF, making the UKF more favorable. Quantitative measurement of the rms error produced by the UKF and EKF for a single-phase system is illustrated in Table 3.

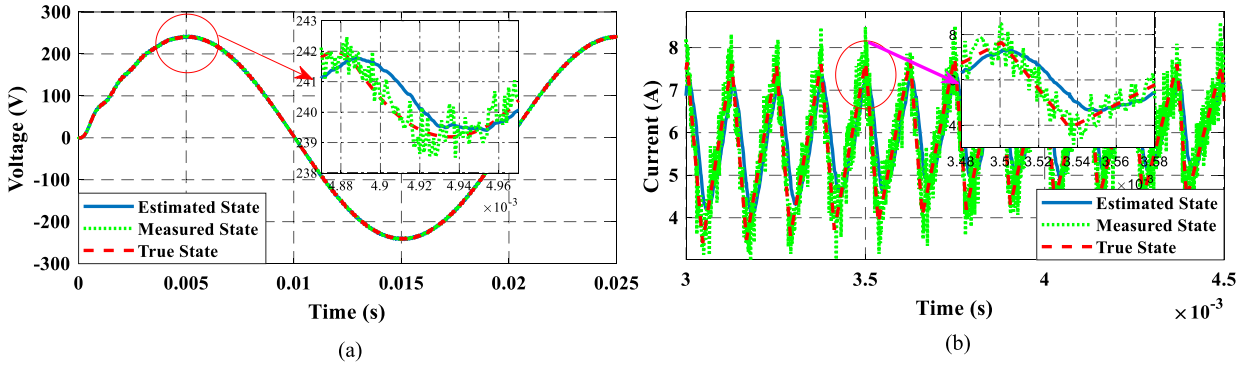

FIGURE 6. (a) Grid voltage and its estimation, (b) inductor current and its estimation using unscented kalman filter.

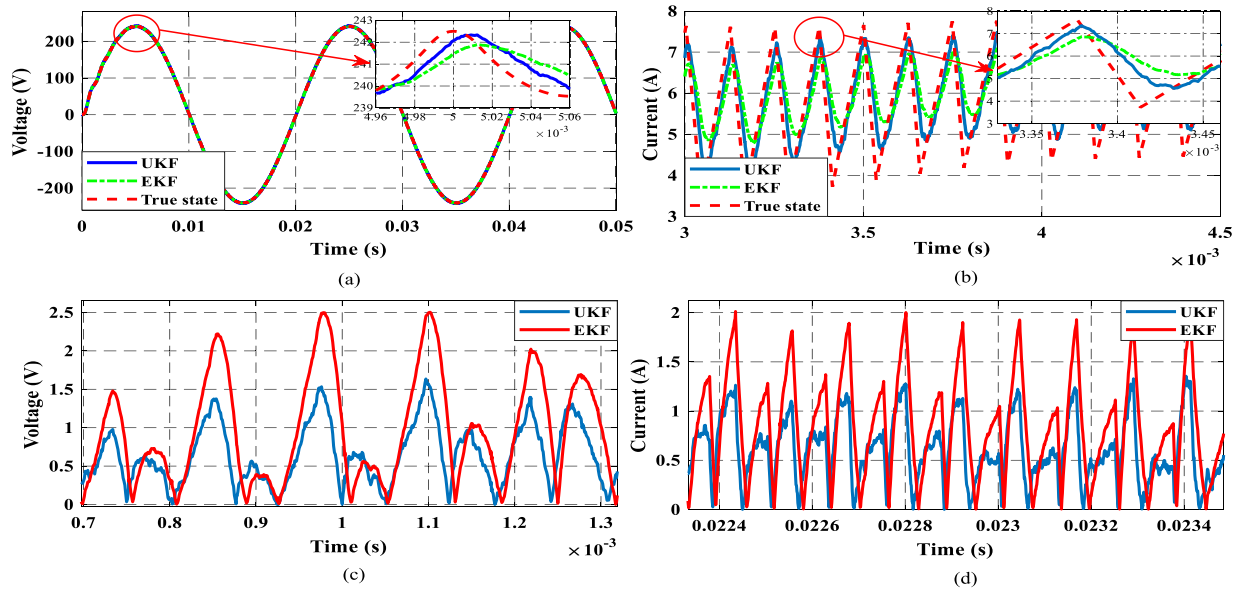

FIGURE 7. Comparison between UKF and EKF for estimating (a) V_g, (b) I_L and error comparison between UKF and EKF in (c) V_g and (d) I_L for single-phase microgrid system.

TABLE 3. Comparison of error (root mean square value) between UKF and EKF for single-phase microgrid.

States	UKF	EKF
$\tilde{V}_g$	1.67 V	2.50 V
$\tilde{I}_L$	1.41 A	2.02 A

2) UKF PERFORMANCE FOR THREE-PHASE SINGLE-SOURCE MICROGRID

In this portion, the state estimation of the three-phase single-source microgrid using the UKF algorithm is presented. The corresponding dq components of grid voltage and current are $\tilde{V}_d$, $\tilde{V}_q$, $\tilde{I}_{t,d}$ and $\tilde{I}_{t,q}$ all of which make up the respective states of the system. The corresponding estimation of these states is given in Fig. 8(a) to 8(d). From the figure, the proposed algorithm is also capable of minimizing the noise and giving a reliable estimation with respect to the true state. The results of the novel UKF algorithm are then compared with the EKF and presented in Fig. 9(a) to 9(d). From this figure, the UKF algorithm is seen to provide a better estimation compared with the EKF algorithm. From Fig. 10, it can also be seen that the use of the UKF results in a lower-estimation error compared with the EKF. Accordingly, a comparative analysis of the rms error generated through the use of the UKF and EKF is presented in Table 4.

TABLE 4. Comparison of error (rms value) between UKF and EKF for three-phase single-source microgrid.

States	UKF	EKF
$\tilde{V}_d$	0.0163 V	0.0824 V
$\tilde{V}_q$	0.061 V	0.135 V
$\tilde{I}_d$	0.83 A	1.72 A
$\tilde{I}_q$	0.89 A	1.78 A

3) UKF PERFORMANCE FOR THREE-PHASE MULTI SOURCE MICROGRID

In this section the performance of the proposed UKF algorithm has been figured out for multiple energy sources.

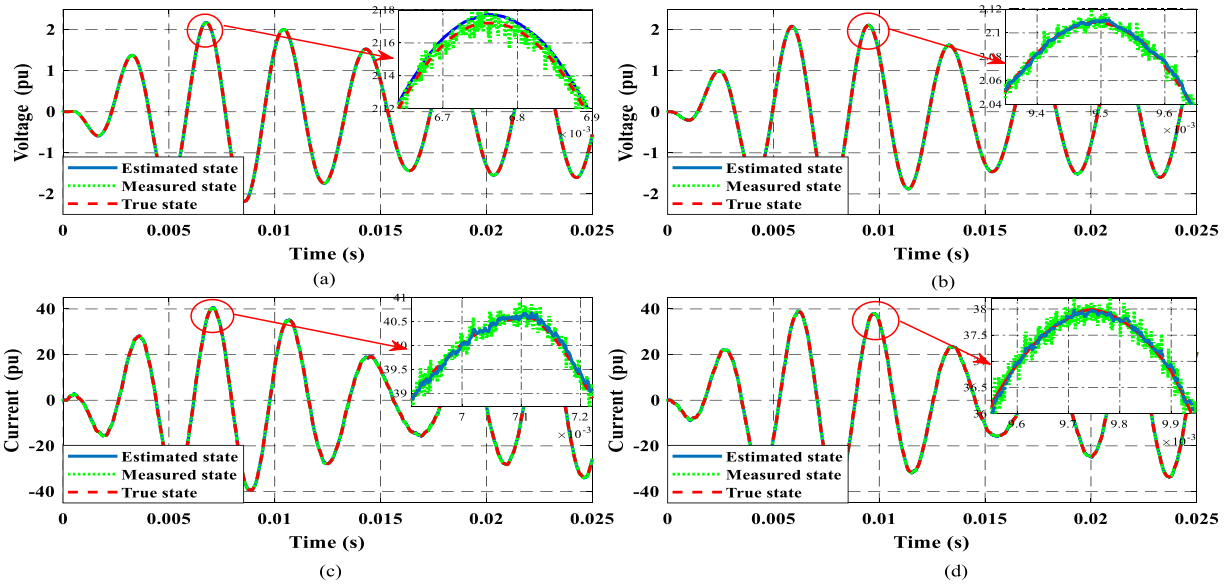

FIGURE 8. (a) d-frame, (b) q-frame voltage and its estimation, (c) d-frame, (d) q-frame current and its estimation for three-phase single-source microgrid using unscented kalman filter.

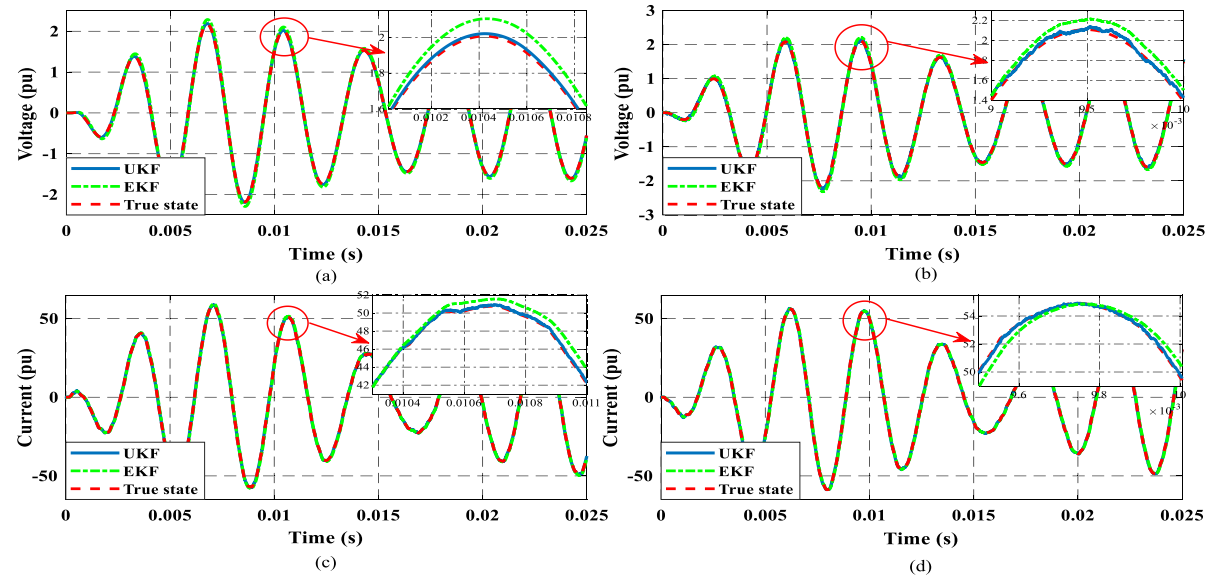

FIGURE 9. Comparison between UKF and EKF for estimating (a) $\tilde{V}_d$, (b) $\tilde{V}_q$, (c) $\tilde{I}_d$ and (d) $\tilde{I}_q$ for three-phase single-source microgrid system.

To make the system two distributed energy resources are connected via point of common coupling. Using the proposed algorithm the d and q components of the corresponding voltage and current are estimated. The corresponding results have been presented in Fig. 11(a) to 11(f). From the simulation results it is seen that the estimated results are obtained from disturbances signals which are closed to the true state. Here, Table 5 also shows the comparative error results between UKF and EKF filter that results claim that the proposed UKF algorithm provides better tracking performance compare with the EKF algorithm.

B. FAULT ANALYSIS

The performance of a microgrid system depends largely on various factors. Deviation in these factors can cause a system to malfunction. Due to such a malfunctioning, a faulty condition can appear in the system at any time. Therefore, it is clear that a novel estimator should estimate the faulty condition that may appear in the system. It is necessary to estimate such a fault in order to provide the signal necessary for the control unit to take the primary initiatives in overcoming this condition. The novelty of the proposed UKF algorithm for the fault condition is justified in this section.

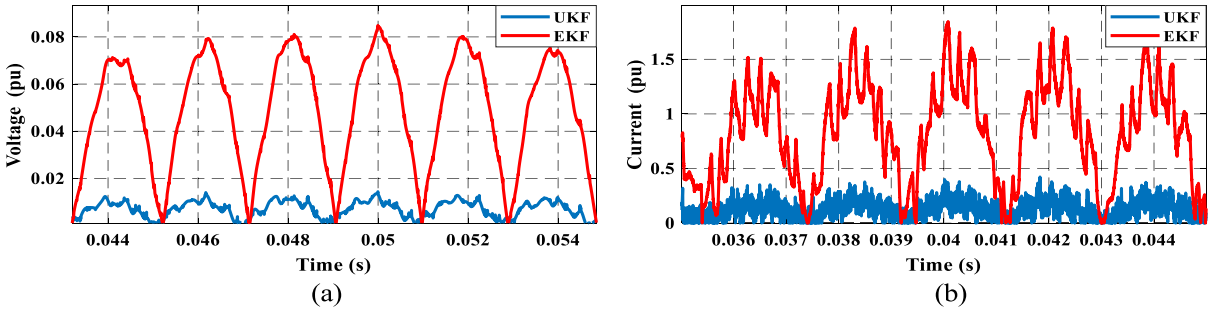

FIGURE 10. Error comparison between UKF and EKF for estimating (a) voltage and (b) current for three-phase single-source microgrid system.

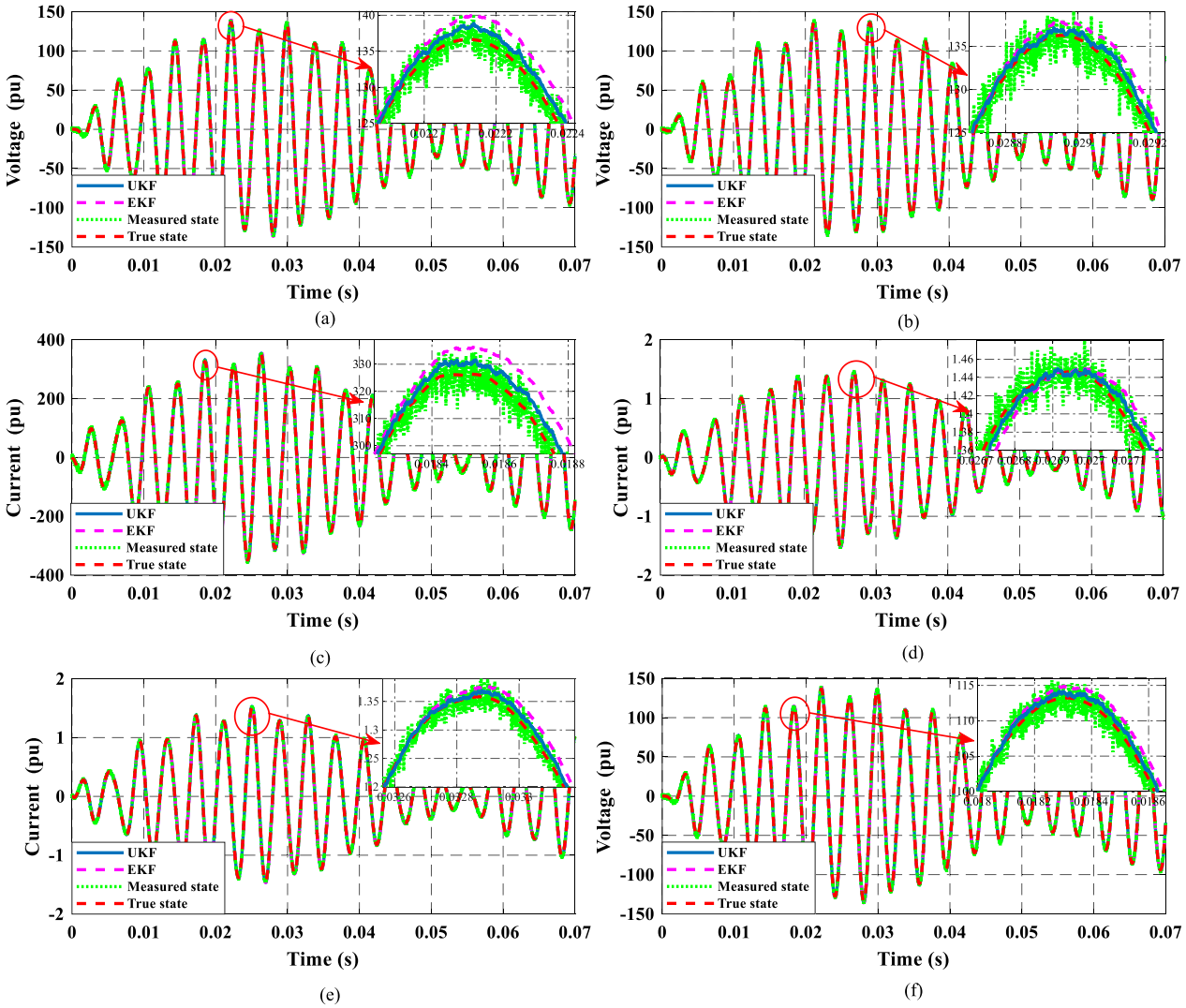

FIGURE 11. (a) $\tilde{V}_{x,d}$, (b) $\tilde{V}_{x,q}$, (c) $\tilde{I}_{tx,q}$, (d) $\tilde{I}_{xy,d}$, (e) $\tilde{I}_{yx,d}$, and (f) $\tilde{V}_{y,q}$ and its estimation using extended and unscented kalman filter.

The analysis was performed for a single-phase, three-phase single-source and three-phase multi-source microgrid system. To substantiate these criteria, the fault condition was applied in the system and the voltage and current deviation during the fault was measured. The effectiveness of the filter is shown in Fig. 12(a), 12(b), and 12(c), respectively, for the fault voltage condition against the single-phase, three-phase single-source, and three-phase multi-source microgrid system. The performance of the UKF filter against the current fault condition is shown in Fig. 12(d), 12(e) and 12(f), respec-

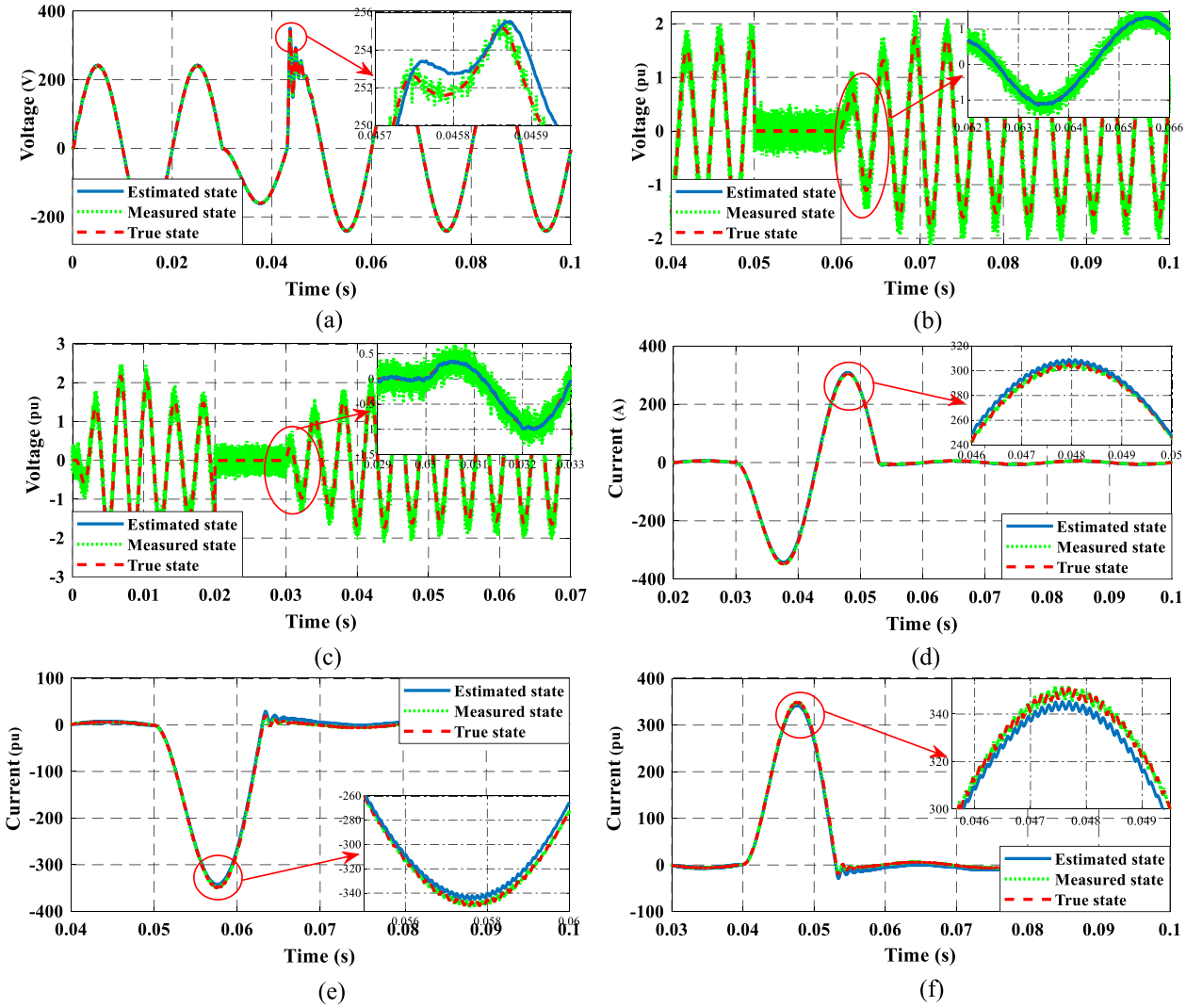

FIGURE 12. Fault voltage analysis for (a) single-phase, (b) three-phase single-source, and (c) three-phase multi-source microgrid. Fault current analysis for (d) single-phase, (e) three-phase single-source, and (f) three-phase multi-source microgrid.

TABLE 5. Comparison of error (rms value) between UKF and EKF for three phase multi source microgrid.

States	UKF	EKF
$\tilde{V}_{x,d}$	0.83 V	1.60 V
$\tilde{V}_{x,q}$	0.78 V	1.52 V
$\tilde{I}_{tx,d}$	1.44 A	2.48 A
$\tilde{I}_{tx,q}$	1.18 A	2.12 A
$\tilde{I}_{xy,d}$	0.23 A	0.41 A
$\tilde{I}_{xy,q}$	0.17 A	0.38 A
$\tilde{I}_{yx,d}$	0.16 A	0.34 A
$\tilde{I}_{yx,q}$	0.18 A	0.37 A
$\tilde{V}_{y,d}$	0.48 V	1.13 V
$\tilde{V}_{y,q}$	0.68 V	1.17 V
$\tilde{I}_{ty,d}$	1.41 A	2.52 A
$\tilde{I}_{ty,q}$	1.48 A	2.63 A

tively. From these figures, it is observed that the UKF filter has the ability to estimate the true state in a fault condition, making the use of this filter a superior method.

C. CONTROLLER PERFORMANCE AGAINST SINGLE-PHASE MICROGRID SYSTEM

An adaptive PID controller was blended into the system to control its voltage and current. The controller performance was then measured against the number of loads, such as a consumer, harmonic, asynchronous-machine and dynamic load. A schematic diagram of these loads is presented in Fig. 13(a) to 13(d), respectively. The results obtained from the investigation are presented in the following section. The results demonstrate the capability of the novel controller to provide a higher-tracking performance with the inclusion of the proposed UKF estimating filter when compared with no filtering method integrated into the system.

1) UNDER SINGLE-PHASE CONSUMER LOAD

A circuit diagram of a single-phase consumer load is shown in Fig. 13(a). DC 300 V is considered the supply voltage while the capacitance and inductance are taken as $C = 15\ \mu F$ and $L = 2\ mH$, respectively. The line

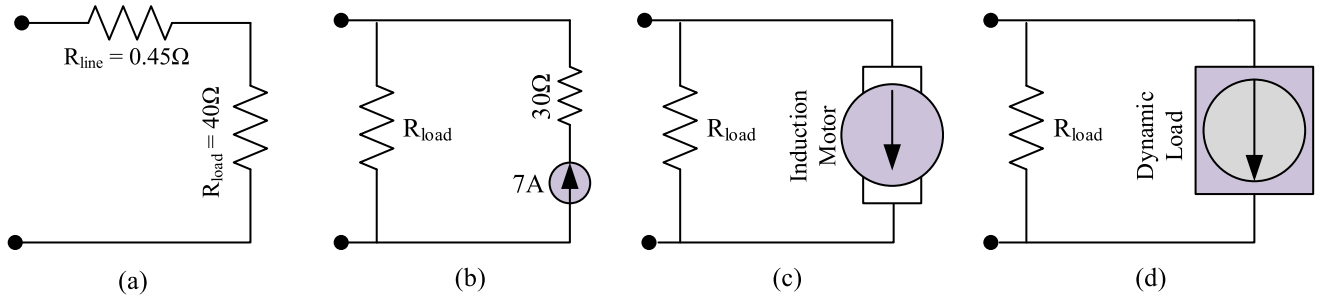

FIGURE 13. Single-phase (a) consumer load, (b) harmonic load, (c) asynchronous machine load and (d) dynamic load.

resistance is chosen as 0.45 Ω and the load resistance as 40 Ω. The proposed method's performance against the consumer load to control voltage and current is illustrated in Fig. 14(a) and 14(e), respectively. The novelty of the controller is compared upon the inclusion of the filter. Using the same value as the controller parameter, the performance is measured once without the integration of the UKF and once with it in a noisy system. From the simulation results, the controller is shown to provide better voltage and current-tracking when integrated with the proposed UKF compared with the use of the controller without the filter.

2) UNDER SINGLE-PHASE HARMONIC LOAD

A diagram of a single phase harmonic load is shown in Fig. 13(b). Appliances such as a television, printer, fluorescent light, computer, transistor, and rectifier serve as nonlinear loads that create voltage and current harmonics in a power system. The use of these loads is increasing on a daily basis. The harmonics generated by these loads cause overheating of the power-system equipment. Connected to the system in a parallel manner, a 7*A* current source with a frequency of 150 *Hz* is considered the harmonic load. The performance against this harmonic load for the voltage and current control is shown in Fig. 14(b) and 14(f), respectively. From these figures, the controller is shown to provide a better-tracking performance when integrated with the UKF. The filter eliminates noise from the system and generates a better signal in terms of the controller and, therefore, the controller is then able to produce a reliable performance against a noisy system.

3) UNDER SINGLE-PHASE ASYNCHRONOUS MACHINE LOAD

A schematic of a single-phase asynchronous machine load is shown in Fig. 13(c) where an induction motor is taken as the load and connected in a parallel manner to the grid. Containing a zero steady state condition, it is modeled as a dq stator reference frame. The active and reactive power of the asynchronous-machine load changes continuously while it is running. Changes the power of the load affects the power of the system, causing the grid to perform poorly. The novel method promotes the tracking activity of the system by lessening the voltage and current oscillation. The novelty of the controller in terms of the voltage and current control is compared with the integration of the UKF in the system and the results are shown in Fig. 14(c) and 14(g), respectively. From the figures, it is evident the controller alone is not efficient enough to produce a reliable tracking performance by reducing the noise.. However, it exhibits a much better tracking performance in a noisy system when the UKF is also included. The filter helps to estimate the true state with respect to the controller and, therefore, the controller is capable of producing improved tracking performance.

4) UNDER SINGLE-PHASE DYNAMIC LOAD

A dynamic load is used in the microgrid system to investigate the novelty of the controller (see diagram in Fig. 13(d)). The load is designed with a current source that possesses active and reactive power at 50 MW and 25 MW, respectively. Variation in this active and reactive power in the voltage of the system considerably affects the performance of the microgrid. The novelty of the controller against the dynamic load is measured in this section and the simulation results for the voltage and current control are shown in Fig. 14(d) and 14(h), respectively. The performance is compared to the integration of the UKF into the system. From these figures, the controller is shown to provide a better tracking performance in a noisy system when the UKF is integrated.

D. CONTROLLER PERFORMANCE AGAINST THREE-PHASE SINGLE-SOURCE MICROGRID SYSTEM

An increase in a subsystem of the microgrid diminishes its performance. Each subsystem comprises different types of energy sources that increase the controlling parameter of the system. Consequently, controlling the three-phase system is much more challenging when compared to a single-phase system. The performance of the controller with the integration of the UKF against the three-phase system is investigated in this section. A schematic of the different types of three-phase loads is presented in Fig. 15. The results of the investigation are outlined in the following section. From these, it is clear that the controller provides a reliable performance when it is included with the UKF.

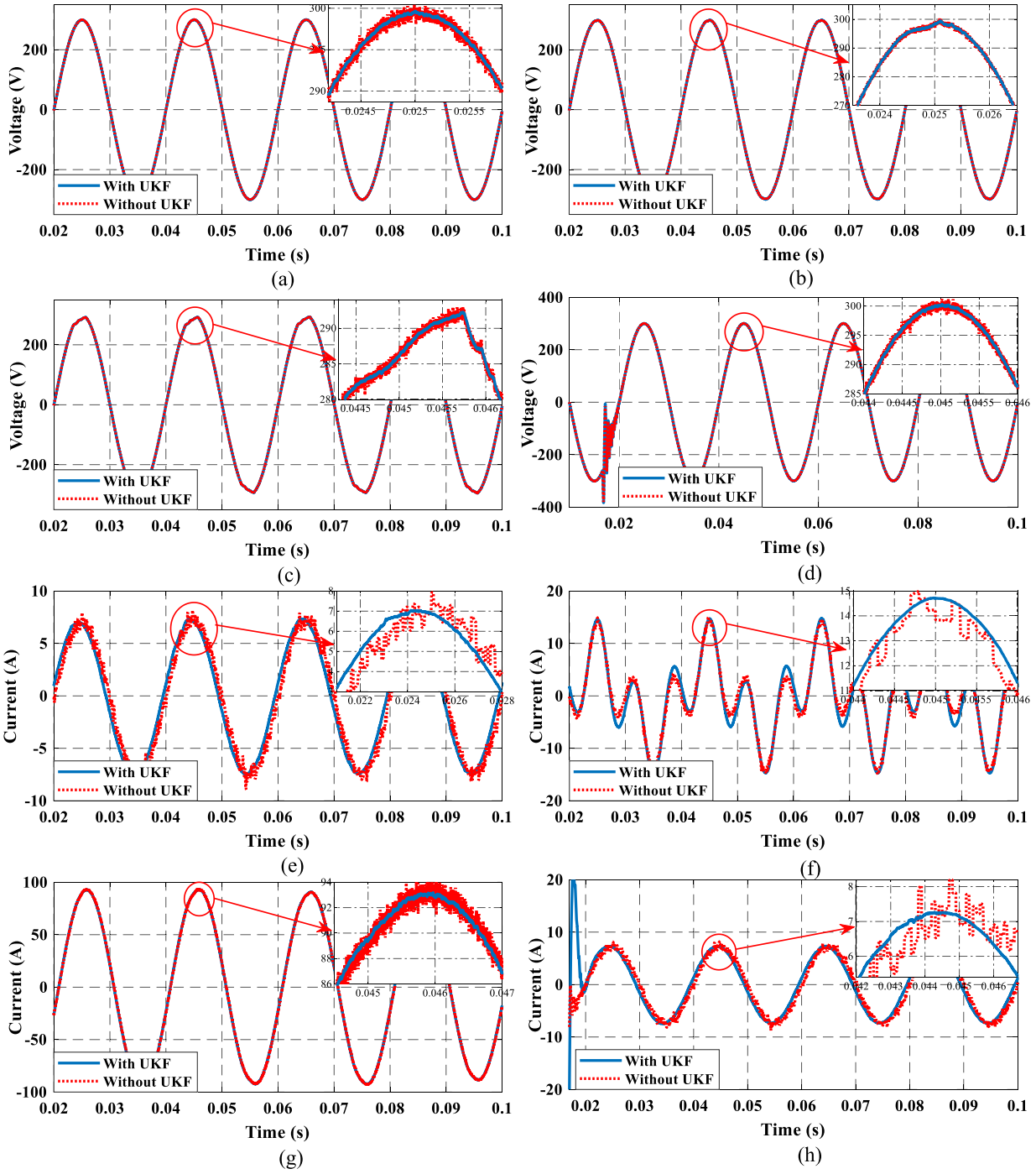

FIGURE 14. Grid voltage control with and without UKF for single-phase (a) consumer, (b) harmonic, (c) asynchronous machine and (d) dynamic load. Current control with and without UKF for single-phase (e) consumer, (f) harmonic, (g) asynchronous machine and (h) dynamic load.

1) UNDER THREE-PHASE SINGLE-SOURCE CONSUMER LOAD

To investigate the novelty of the controller for a three-phase system, a three-phase consumer load is modeled, as shown in Fig. 15(a). The initial reference voltage is taken as $V_d = 0.8pu$ and $V_q = 0.6pu$. The performance of the controller against a three-phase consumer load is measured in this section and the results of the simulation are detailed in Fig. 16(a) and 16(b) in terms of voltage and current control respectively. The novelty of the controller is also compared with the inclusion of the UKF in a noisy system. From these figures, the controller is shown to provide better control of the dq components of the voltage and current when the UKF is integrated.

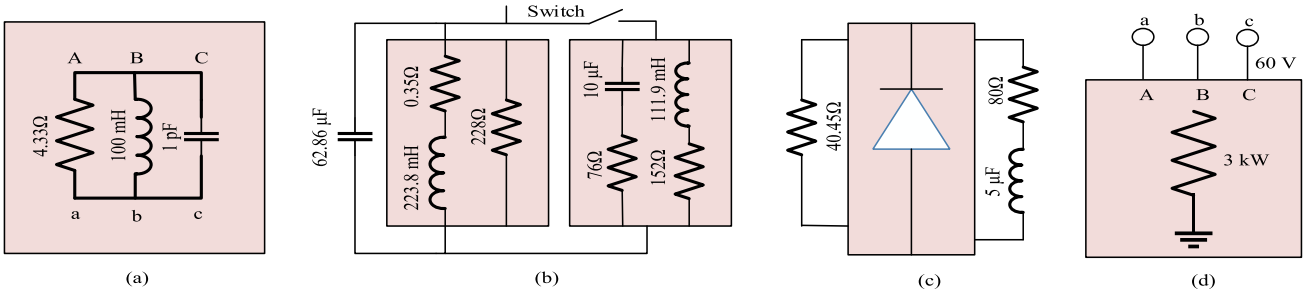

FIGURE 15. Three-phase (a) consumer load, (b) unknown load, (c) nonlinear load and (d) balance load.

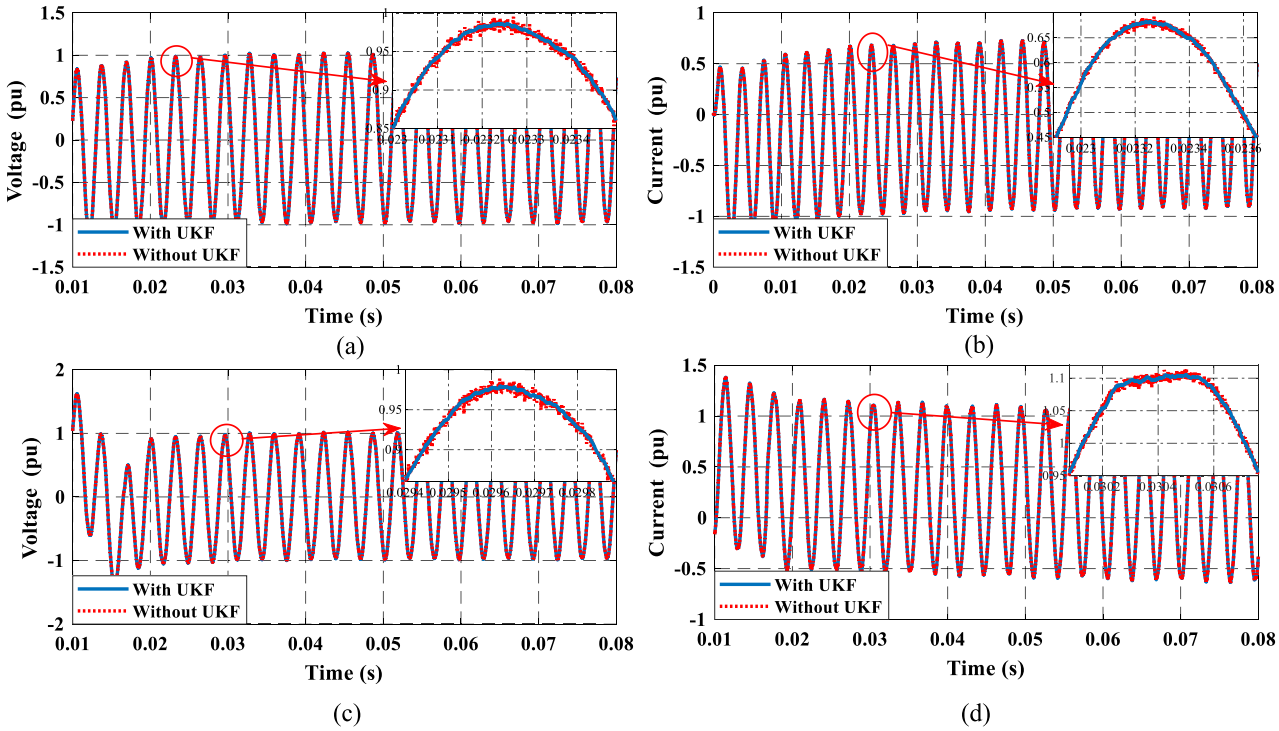

FIGURE 16. (a) Voltage and (b) current control with and without UKF for three-phase single-source consumer load. (c) Voltage and (d) current control with and without UKF for three-phase single-source unknown load.

2) UNDER THREE-PHASE SINGLE-SOURCE UNKNOWN LOAD

A three-phase unknown load is modeled and presented in Fig. 15(b) to measure how reliable the novelty of the controller is. The load comprises resistance, inductance, capacitance and a switch. The inclusion of this load changes the voltage and current of the system, as the activation of the switch modifies the parameter of the load, in turn changing the instantaneous voltage and current. The effectiveness of the controller over the unknown load is presented in Fig. 16(c) and 16(d). The corresponding *dq* components of the voltage and current are controlled by the controller with the integration of the UKF. From the comparative analysis presented in the given figure, the controller is shown to achieve improved control of the voltage and current when it is integrated with the UKF.

3) UNDER THREE-PHASE SINGLE-SOURCE NONLINEAR LOAD

The novelty of the controller against a three phase nonlinear load is shown in this section, as shown in Fig. 15(c). The load consists of a six-pulse diode bridge rectifier which is connected in a parallel manner with the grid. The results of the controller against this nonlinear load are evaluated in this section and presented in Fig. 17(a) and 17(b). From these figures, the controller is shown to be ineffective in reducing the noise in the system and in providing reliable control over the voltage and current components. However, when the filter is integrated into the system, the effectiveness of the controller increases, as the UKF helps to achieve the true state of the system requiring control.

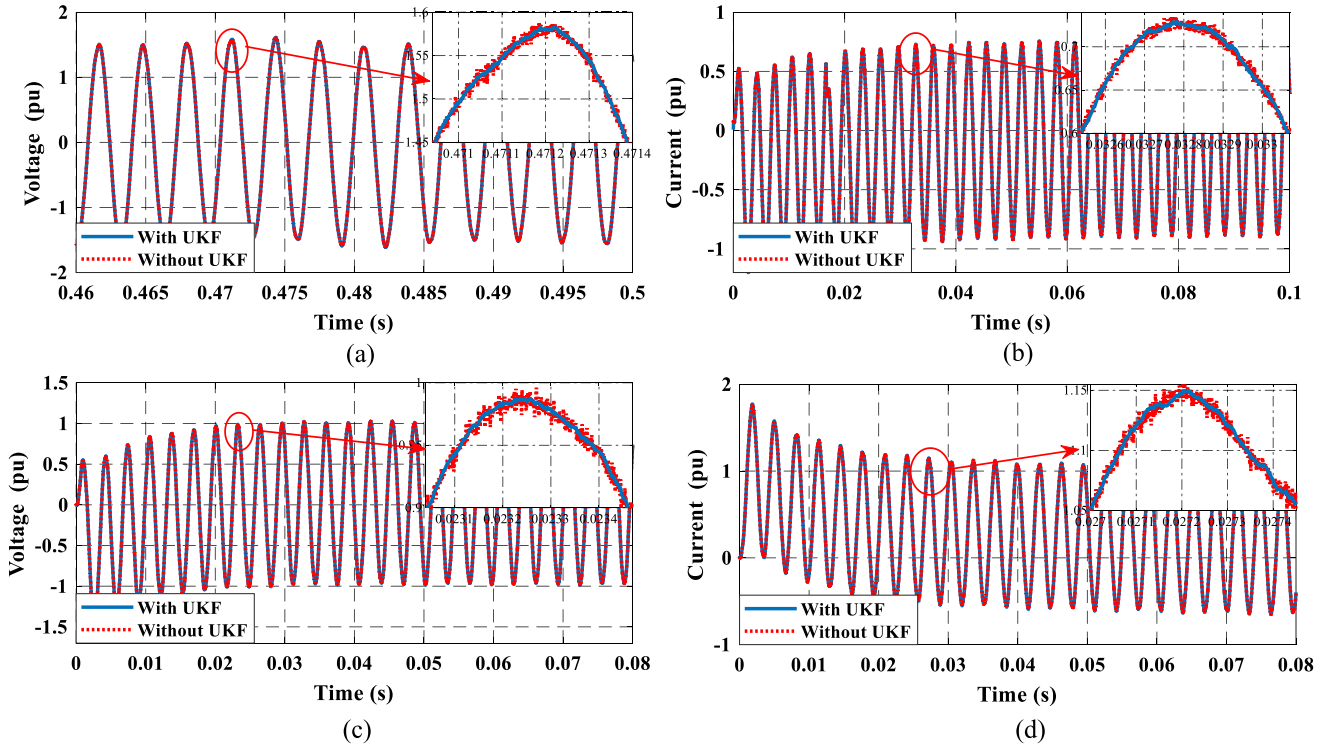

FIGURE 17. (a) Voltage and (b) current control with and without UKF for three-phase single-source nonlinear load. (c) Voltage and (d) current control with and without UKF for three-phase single-source balance load.

4) UNDER THREE-PHASE SINGLE-SOURCE BALANCE LOAD

A schematic diagram of a three-phase balanced load is given in Fig. 15(d). This section shows the novelty of the controller against balanced load. The load is modeled using a resistive load with the active power of 3 kW and a nominal phase-to-phase voltage of 60 V. The dq components of the voltage and the current of the load are controlled and the results are presented in Fig. 17(c) and 17(d). The performance of the controller is evaluated once without the inclusion of the UKF and once with it. From Fig. 17, the controller is shown to provide better control over the system when the UKF is used compared to without it.

E. CONTROLLER PERFORMANCE AGAINST THREE-PHASE MULTI-SOURCE MICROGRID SYSTEM

As the number of energy sources increases, the controlling of microgrid becomes more daunting. That's why controlling the three phase multi DGs based microgrid system is more complicated than three phase single source microgrid system. The novelty of the controller with the integration of the UKF filter in three phase multi DGs based microgrid system is investigated in this section against different types of loads. The following section presents the obtained results of the investigation that ensures that the proposed controller included with the UKF provides reliable performance.

1) UNDER THE THREE-PHASE MULTI-SOURCE CONSUMER LOAD

For a three-phase multi DGs based MG system, a three phase consumer load is modeled as shown in Fig. 15(a) to investigate the performance of the controller. Here the reference voltages V_d and V_q are taken as initially 0.8 and 0.6 respectively. The novelty of the controller is evaluated in this section against three phase consumer load and the simulation results are shown in Fig.18(a) and 18(e). From the figure, it is seen that the controller with a filter provides better control of the dq components for the voltage and current.

2) UNDER THREE-PHASE MULTI-SOURCE UNKNOWN LOAD

Fig. 15(b) represents the model of a three-phase unknown load that is used to check the novelty of the controller for the unknown condition. For the unknown load basically resistance, capacitance, inductance and switch are used. The voltage and current of the system changes due to the activation of the switch that changes the parameter of the load. The effectiveness of the controller over the unknown load is presented in Fig. 18(b) and 18(f). The voltage and current corresponding the dq components are controlled by the controller which is integrated with the UKF filter. From the figure it is seen that the integration of UKF with the controller provides better tracking of voltage and current.

3) UNDER THREE-PHASE MULTI-SOURCE NONLINEAR LOAD

The effectiveness of the novel controller against three phase nonlinear load is shown in this section which is modeled as shown in Fig. 15(c). The six pulse diode bridge is used to model the nonlinear load which is connected in parallel with the grid. The novelty of the controller is evaluated in

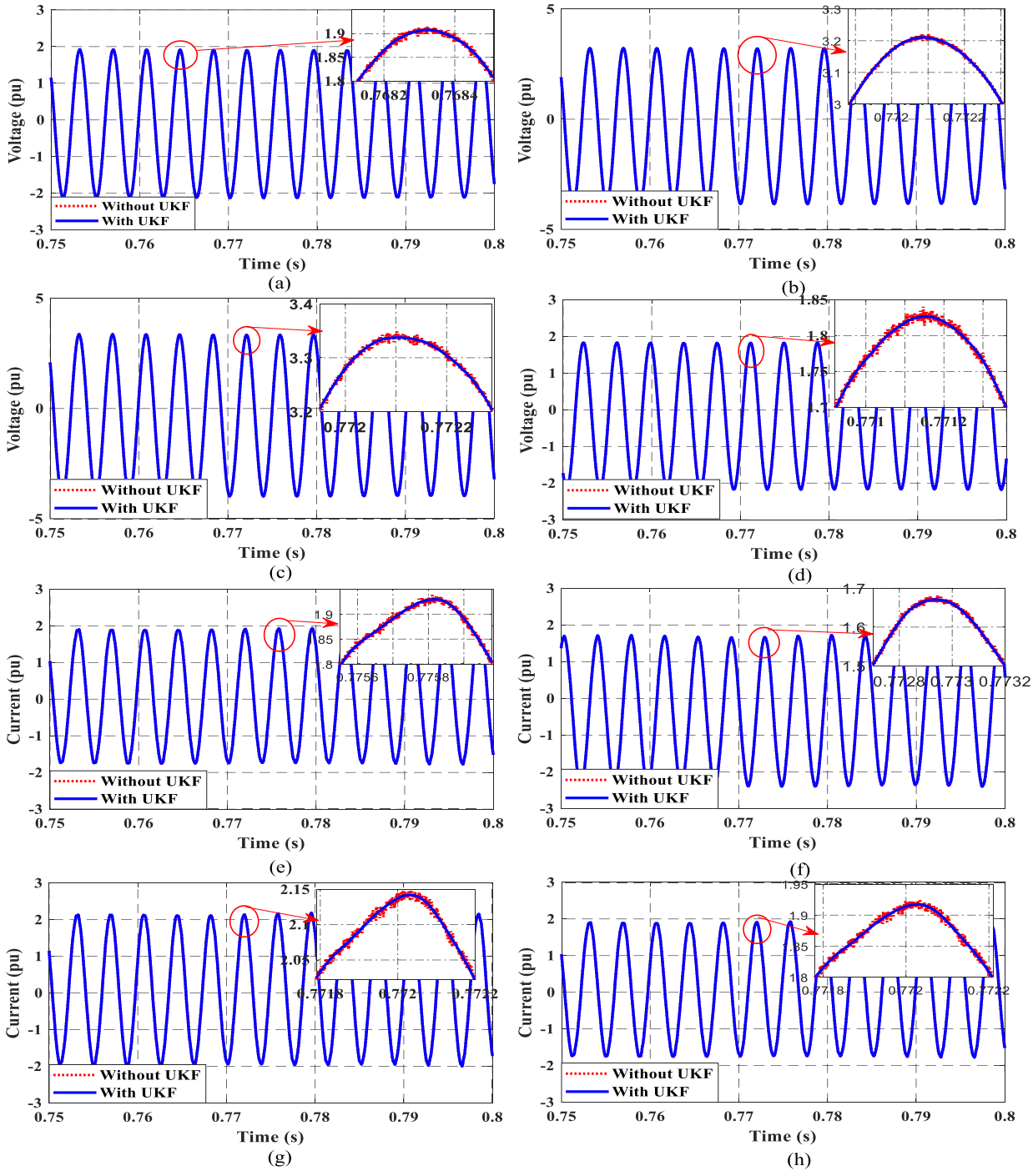

FIGURE 18. Voltage control with and without UKF for three-phase multi-source (a) consumer, (b) unknown, (c) nonlinear and (d) balance load. Current control with and without UKF for three-phase multi-source (e) consumer, (f) unknown, (g) nonlinear and (h) balance load.

this section against nonlinear load and the result is presented in Fig. 18(c) and 18(g). It is shown in the figure, the controller is not capable of reducing noise from the system and to generate a reliable state. But the integration of the filter with the controller creates the ability of the controller to reduce the noise from the signals and generates a reliable state of the system that has to be controlled.

4) UNDER THREE-PHASE MULTI-SOURCE BALANCE LOAD

Fig. 15(d) shows the schematic diagram of the three phase balanced load. The effectiveness of the controller is evaluated for balance load. A resistive load with the active power of 3 kW and nominal phase to phase voltage of 60 V are used to model the load. The dq components of the voltage and current of the load are controlled. The obtained results are

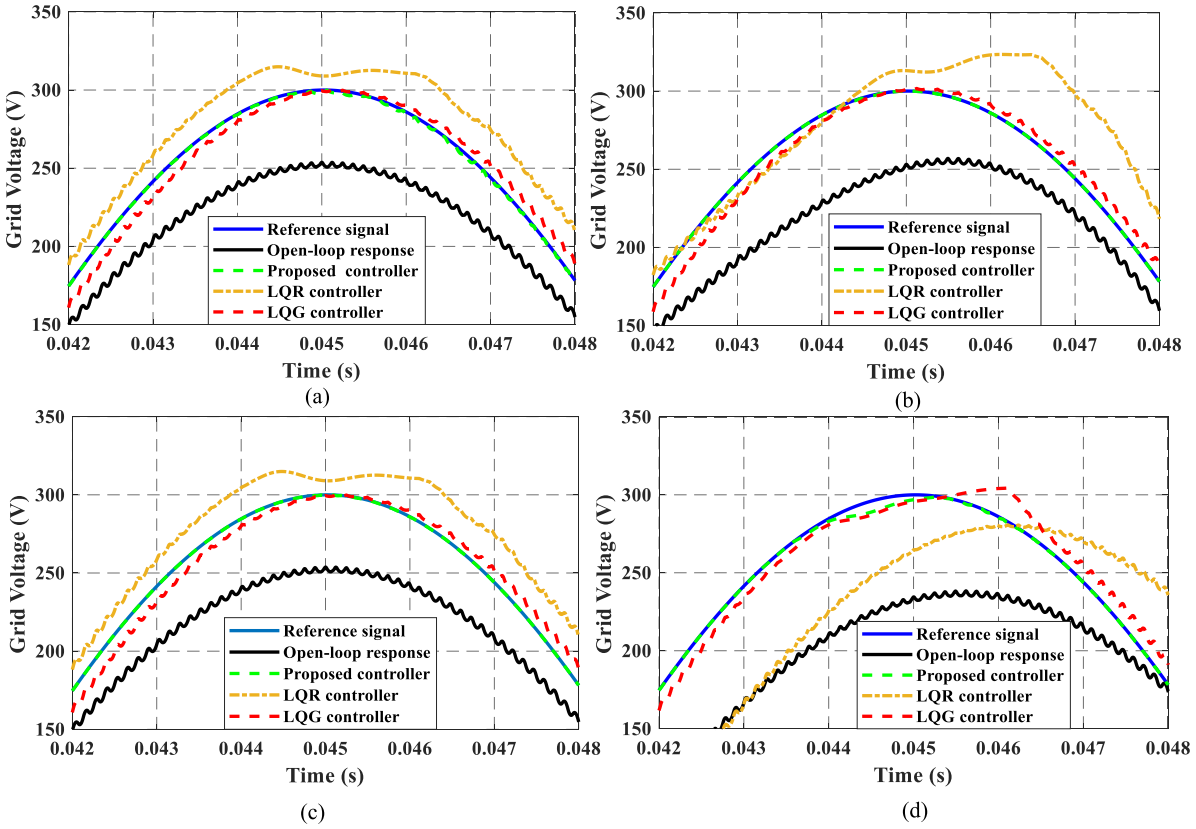

FIGURE 19. Performance comparison for (a) consumer, (b) harmonic, (c) asynchronous machine, and (d) dynamic load between proposed controller, LQR, and LQG.

shown in Fig. 18(d) and 18(h). The performance of the UKF algorithm is evaluated both integrated controller and without integrating controller. It is seen that when the controller is added to the system with the UKF algorithm then better results are obtained.

F. COMPARATIVE PERFORMANCE ANALYSIS AMONG DIFFERENT CONTROLLERS

In order to verify the superior performance of the proposed controller, its performance is compared with linear quadratic regulator (LQR) and linear quadratic gaussian (LQG) controller. The obtained results are described in Fig. 19(a) to 19(d) for consumer, harmonic, asynchronous machine, and dynamic load, respectively. From these figures, it is evident that the proposed controller shows better tracking performance with compared to the linear quadratic regulator and linear quadratic gaussian controller. A quantitative comparison of these controllers are presented in Table 6 from which it is also obvious that the proposed controller generates less error with compared to LQR and LQG controller that assures high performance of it.

G. ROBUSTNESS ANALYSIS

In order to show the robustness of the proposed control technique, several filter capacitor values for single DG single-phase microgrid were taken and the performance of the controller against such values was measured. As shown

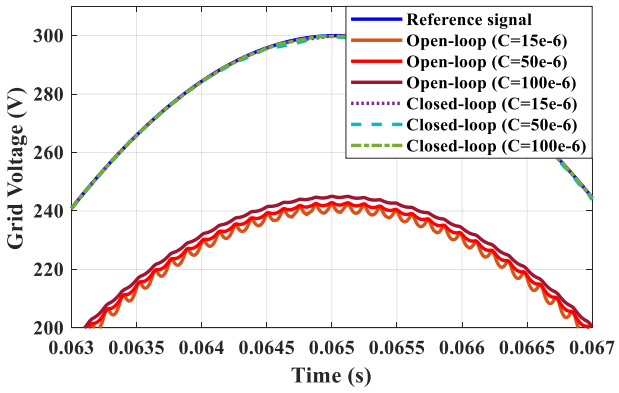

FIGURE 20. Robustness analysis of the proposed controller.

in Fig. 20, it is seen that controller performance remains stable and accurate to the reference with the change in plant dynamics that ensures the performance robustness and stability of the controller against changes in plant dynamics.

H. DISCUSSION AND ACHIEVEMENTS

The proposed blended state estimated adaptive controller is investigated against the number of load dynamics. A change in load dynamics creates an unknown environment, ultimately causing poor performance of the system. In this work, we present the design of a novel blended state estimated adaptive control technique that firstly estimates the true state of the microgrid at noisy situations and provides extensive control

TABLE 6. Error voltages (rms value) comparison using the proposed controller, LQR, and LQG controller.

Name of controller	Error voltage for consumer load (V)	Error voltage for harmonic load (V)	Error voltage for asynchronous machine load (V)	Error voltage for dynamic load (V)
Proposed controller	2.53	3.13	6.88	2.44
LQR controller	23.2	30.1	77.43	23.1
LQG controller	11.2	11.55	18.53	13,38

of voltage and current for such variations of load dynamics. The results given in the figures demonstrate the robust performance of the controller with the inclusion of the UKF in the system. The UKF provides the state of the system closest to the true state, helping the controller to achieve better tracking of the voltage and current for both single and three-phase microgrid systems. The effectiveness of the proposed controller is also evaluated against different load dynamics and controllers. For the consumer load the proposed controller generates 2.53 error voltage where the LQR and the LQG controller generate 23.2 and 11.2 error voltage respectively. The error voltages for harmonic load, asynchronous machine load and dynamic load are shown in Table 6. From these error voltages it is concluded that the proposed controller is more effective than LQR and LQG controller.

V. CONCLUSION

A novel blended state estimated adaptive controller is designed in this paper to improve the high performance control of voltage and current for multi DG islanded microgrid against unknown loads and faults. The problem statement of voltage and current control of microgrid has been extended to incorporate the effect of system noise in the form of packet losses and disturbances. The controller was developed for single-phase, three-phase single-source and three-phase multi-source microgrid and the performance was compared with the LQR and LQG controller. The results validate the use of the proposed method ensures the accuracy of state estimation as well as the voltage and current control of the system. The performance of the controller was simulated against a number of load dynamics for both single and three-phase systems. The results show the controller provides a more reliable performance as compared with LQR and LQG controller for different load dynamics to ensure the extensive performance of it. The future research direction of this study maybe extended to the estimation of the state and control of voltage, current, and power of the microgrid integrating with the main grid as well as balancing the frequency of the system.

REFERENCES

[1] S. Parhizi, H. Lotfi, A. Khodaei, and S. Bahramirad, "State of the art in research on microgrids: A review," *IEEE Access*, vol. 3, pp. 890–925, 2015.

[2] M. Babazadeh and H. Karimi, "A robust two-degree-of-freedom control strategy for an islanded microgrid," *IEEE Trans. Power Del.*, vol. 28, no. 3, pp. 1339–1347, Jul. 2013.

[3] S. K. Das, M. Rahman, S. K. Paul, M. Armin, P. N. Roy, and N. Paul, "High-performance robust controller design of plug-in hybrid electric vehicle for frequency regulation of smart grid using linear matrix inequality approach," *IEEE Access*, vol. 7, pp. 116911–116924, 2019.

[4] A. Kumar, A. R. Singh, Y. Deng, X. He, P. Kumar, and R. C. Bansal, "A novel methodological framework for the design of sustainable rural microgrid for developing nations," *IEEE Access*, vol. 6, pp. 24925–24951, 2018.

[5] R. M. Kamel, A. Chaouachi, and K. Nagasaka, "Three control strategies to improve the microgrid transient dynamic response during isolated mode: A comparative study," *IEEE Trans. Ind. Electron.*, vol. 60, no. 4, pp. 1314–1322, Apr. 2013.

[6] F. R. Badal, P. Das, S. K. Sarker, and S. K. Das, "A survey on control issues in renewable energy integration and microgrid," *Protection Control Mod. Power Syst.*, vol. 4, no. 1, p. 8, 2019.

[7] M. Akter, M. A. Rahman, M. S. Munsi, A. B. Siddique, S. K. Sarkar, and S. K. Das, "Multi-objective model reference modified adaptive PID framework to islanded microgrid control under various load conditions," in *Proc. Int. Conf. Adv. Elect. Electron. Eng. (ICAEEE)*, Nov. 2018, pp. 1–4.

[8] S. K. Sarkar, M. H. K. Roni, D. Datta, S. K. Das, and H. R. Pota, "Improved design of high-performance controller for voltage control of islanded microgrid," *IEEE Syst. J.*, vol. 13, no. 2, pp. 1786–1795, Jun. 2019.

[9] K. T. Tan, B. Sivaneasan, X. Y. Peng, and P. L. So, "Control and operation of a DC grid-based wind power generation system in a microgrid," *IEEE Trans. Energy Convers.*, vol. 31, no. 2, pp. 496–505, Jun. 2016.

[10] Y. Liu, A. P. S. Meliopoulos, R. Fan, L. Sun, and Z. Tan, "Dynamic state estimation based protection on series compensated transmission lines," *IEEE Trans. Power Del.*, vol. 32, no. 5, pp. 2199–2209, Oct. 2017.

[11] E. Mengelkamp, J. Gärttner, K. Rock, S. Kessler, L. Orsini, and C. Weinhardt, "Designing microgrid energy markets: A case study: The Brooklyn Microgrid," *Appl. Energy*, vol. 210, pp. 870–880, Jan. 2018.

[12] J. Zhao, G. Zhang, Z. Y. Dong, and M. L. Scala, "Robust forecasting aided power system state estimation considering state correlations," *IEEE Trans. Smart Grid*, vol. 9, no. 4, pp. 2658–2666, Jul. 2018.

[13] C. Xu and A. Abur, "A fast and robust linear state estimator for very large scale interconnected power grids," *IEEE Trans. Smart Grid*, vol. 9, no. 5, pp. 4975–4982, Sep. 2018.

[14] D. Datta, M. R. I. Sheikh, S. K. Sarkar, and S. K. Das, "Robust positive position feedback controller for voltage control of islanded microgrid," *Energy*, vol. 1, p. 3, Jul. 2018.

[15] S. Kamireddy, N. N. Schulz, and A. K. Srivastava, "Comparison of state estimation algorithms for extreme contingencies," in *Proc. 40th North Amer. Power Symp.*, Sep. 2008, pp. 1–5.

[16] C. Gomez-Quiles, A. Gomez-Exposito, and A. de la Villa Jaen, "State estimation for smart distribution substations," *IEEE Trans. Smart Grid*, vol. 3, no. 2, pp. 986–995, Jun. 2012.

[17] L. Reggiani, L. Dossi, L. Barletta, and A. Spalvieri, "Extended Kalman filter for MIMO phase noise channels with independent oscillators," *IEEE Commun. Lett.*, vol. 22, no. 6, pp. 1200–1203, Jun. 2018.

[18] S. Yu, K. Emami, T. Fernando, H. H. C. Iu, and K. P. Wong, "State estimation of doubly fed induction generator wind turbine in complex power systems," *IEEE Trans. Power Syst.*, vol. 31, no. 6, pp. 4935–4944, Nov. 2016.

[19] P. Liu, Y.-P. Tian, and Y. Zhang, "Distributed Kalman filtering with finite-time max-consensus protocol," *IEEE Access*, vol. 6, pp. 10795–10802, 2018.

[20] R. Olfati-Saber, "Kalman-consensus filter: Optimality, stability, and performance," in *Proc. 48th IEEE Conf. Decis. Control (CDC) Jointly 28th Chin. Control Conf.*, Dec. 2009, pp. 7036–7042.

[21] K. Emami, T. Fernando, H. H. C. Iu, H. Trinh, and K. P. Wong, "Particle filter approach to dynamic state estimation of generators in power systems," *IEEE Trans. Power Syst.*, vol. 30, no. 5, pp. 2665–2675, Sep. 2015.

[22] F. Wang, J. Zhang, B. Lin, and X. Li, "Two stage particle filter for nonlinear Bayesian estimation," *IEEE Access*, vol. 6, pp. 13803–13809, 2018.

[23] A. Ahmed, M. Moinuddin, and U. M. Al-Saggaf, "State space least mean fourth algorithm for dynamic state estimation in power systems," *Arabian J. Sci. Eng.*, vol. 41, no. 2, pp. 527–543, 2016.
[24] M. B. Malik and M. Salman, "State-space least mean square," *Digit. Signal Process.*, vol. 18, no. 3, pp. 334–345, 2008.
[25] J. Ni and F. Li, "A variable step-size matrix normalized subband adaptive filter," *IEEE Trans. Audio, Speech, Language Process.*, vol. 18, no. 6, pp. 1290–1299, Aug. 2010.
[26] Q. L. Lam, A. I. Bratcu, D. Riu, and J. Mongkoltanatas, "Multi-variable h-infinity robust control applied to primary frequency regulation in microgrids with large integration of photovoltaic energy source," in *Proc. IEEE Int. Conf. Ind. Technol. (ICIT)*, Mar. 2015, pp. 2921–2928.
[27] J. Mongkoltanatas, D. Riu, and X. LePivert, "H infinity controller design for primary frequency control of energy storage in islanding microgrid," in *Proc. 15th Eur. Conf. Power Electron. Appl. (EPE)*, Sep. 2013, pp. 1–11.
[28] J. M. Wassick, P. S. McCroskey, J. J. McDonough, and D. K. Steckler, "Model predictive controller," U.S. Patent 574 003 3A, Apr. 14, 1998.
[29] N. Yang, D. Li, J. Zhang, and Y. Xi, "Model predictive controller design and implementation on FPGA with application to motor servo system," *Control Eng. Pract.*, vol. 20, no. 11, pp. 1229–1235, 2012.
[30] M. Ghafouri, U. Karaagac, H. Karimi, S. Jensen, J. Mahseredjian, and S. O. Faried, "An LQR controller for damping of subsynchronous interaction in DFIG-based wind farms," *IEEE Trans. Power Syst.*, vol. 32, no. 6, pp. 4934–4942, Nov. 2017.
[31] S. K. Sarker, F. R. Badal, P. Das, and S. K. Das, "Multivariable integral linear quadratic Gaussian robust control of islanded microgrid to mitigate voltage oscillation for improving transient response," *Asian J. Control*, vol. 21, no. 4, pp. 2114–2125, 2019.
[32] T. L. Vandoorn, B. Renders, L. Degroote, B. Meersman, and L. Vandevelde, "Voltage control in islanded microgrids by means of a linear-quadratic regulator," in *Proc. IEEE Benelux Young Res. Symp. Elect. Power Eng. (YRS)*, Leuven, Belgium, Mar. 2010, pp. 1–5.
[33] A. B. Siddique, M. S. Munsi, S. K. Sarker, S. K. Das, and M. R. Islam, "Voltage and current control augmentation of islanded microgrid using multifunction model reference modified adaptive PID controller," *Int. J. Elect. Power Energy Syst.*, vol. 113, pp. 492–501, Dec. 2019.
[34] A. B. Siddique, S. Munsi, S. K. Sarkar, and S. K. Das, "Model reference modified adaptive PID controller design for voltage and current control of islanded microgrid," in *Proc. 4th Int. Conf. Elect. Eng. Inf. Commun. Technol. (iCEEiCT)*, Sep. 2018, pp. 130–135.

MD. SHAHIN MUNSI was born in Chandpur, Bangladesh. He received the B.Sc. degree in mechatronics engineering from the Rajshahi University of Engineering & Technology (RUET), Bangladesh, in 2019. He is currently with Control System Research Group, RUET. His research interests include smart grid systems, electric vehicles, electrical machines, robotics, and renewable energy sources.

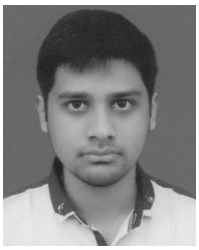

ABU BAKAR SIDDIQUE was born in Chandpur, Bangladesh. He received the B.Sc. degree from the Department of Mechatronics Engineering, Rajshahi University of Engineering & Technology (RUET), Rajshahi, Bangladesh, in 2019. His research interest includes control theory and applications.

SAJAL K. DAS was born in Rajshahi, Bangladesh. He received the Ph.D. degree in electrical engineering from the University of New South Wales, Australia, in 2014. In May 2014, he was appointed as a Research Engineer with the National University of Singapore (NUS), Singapore. In January 2015, he joined the Department of Electrical and Electronic Engineering, American International University Bangladesh (AIUB), as an Assistant Professor. He then joined the Department of Mechatronics Engineering, Rajshahi University of Engineering & Technology (RUET), as a Lecturer, in September 2015, where he is currently the Head of the Department of Mechatronics Engineering. His research interests include control theory and applications, mechatronics system control, robotics, and power system control.

SANJOY KUMAR PAUL received the Ph.D. degree from the University of New South Wales.

He is currently with the UTS Business School, University of Technology Sydney, Australia. He has several years of experiences as an academic. He has published more than 50 articles in top-tier journals and conferences, including the *European Journal of Operational Research*, the *International Journal of Production Economics*, *Computers and Operations Research*, the *International Journal of Production Research*, *Annals of Operations Research*, the *Journal of Management in Engineering*, the *Journal of Cleaner Production*, *Computers and Industrial Engineering*, the *Journal of Retailing and Consumer Services*, and the *Journal of Intelligent Manufacturing*. His research interests include supply chain risk management, modeling, applied operations research, and intelligent decision making. He is a member of the Australian Society for Operations Research (ASOR) and the Australasian Supply Chain Institute (ASCI). He is also a Committee Member of the Industry Risk Committee of ASCI. He received several awards in his career, including the ASOR Rising Star Award, the Excellence in Early Career Research Award from the UTS Business School, the Stephen Fester Prize for most outstanding thesis from UNSW, and the High-Impact Publications Award for publishing articles in top-tier journals. He is a Guest Editor, an Associate Editor, and an Editorial Board Member of several journals. He is also an active Reviewer for many reputed journals.

MD. RABIUL ISLAM (M'14–SM'16) received the B.Sc. and M.Sc. degrees from the Rajshahi University of Engineering & Technology (RUET), Rajshahi, Bangladesh, in 2003 and 2009, respectively, and the Ph.D. degree from the University of Technology Sydney (UTS), Sydney, Australia, in 2014, all in electrical engineering.

He was appointed as a Lecturer at RUET, in 2005, and promoted to Full Professor, in 2017. In early 2018, he joined the School of Electrical, Computer, and Telecommunications Engineering (SECTE), University of Wollongong (UOW), Wollongong, Australia, where he is currently a member of the Australian Power Quality and Reliability Center. He has authored or coauthored 130 articles (including 34 IEEE transaction articles) in international journals and conference proceedings. His research interests include power electronic converters, renewable energy technologies, power quality, electrical machines, electric vehicles, and smart grid. He has served as a Guest Editor for the IEEE TRANSACTIONS ON ENERGY CONVERSION and the IEEE TRANSACTIONS ON APPLIED SUPERCONDUCTIVITY. He is currently an Editor of a special issue for *IET Electric Power Applications*.

MOHAMMAD ALI MONI received the Ph.D. degree in artificial intelligence and machine learning from the University of Cambridge, U.K., in 2014. From 2015 to 2017, he was a Postdoctoral Research Fellow with the Garvan Institute of Medical Research, Sydney, and was an Associate Lecturer with the University of New South Wales, Australia. At the end of 2017, he was awarded the University of Sydney DVC Fellowship. He is also an Assistant Professor with the Department of Computer Science and Engineering, Pabna University of Science & Technology. His research interests include artificial intelligence, machine learning, data science, and clinical bioinformatics.